Chemical Geology 384 (2014) 135–148

Contents lists available at ScienceDirect

Chemical Geology

journal homepage: www.elsevier.com/locate/chemgeo

Metal scavenging by calcium carbonate at the Eyjafjallajökull volcano: A carbon capture and storage analogue

J. Olsson [a,b,*], S.L.S. Stipp [a], E. Makovicky [c], S.R. Gislason [b]

[a] Nano-Science Center, Department of Chemistry, University of Copenhagen, Universitetsparken 5, DK-2100 København Ø, Denmark
[b] Nordic Volcanological Institute, Institute of Earth Sciences, University of Iceland, Sturlugata 7, 101 Reykjavik, Iceland
[c] Department of Geoscience and Natural Resource Management, University of Copenhagen, Øster Voldgade 10, DK-1350 København K, Denmark

ARTICLE INFO

Article history:
Received 10 January 2014
Received in revised form 23 June 2014
Accepted 26 June 2014
Available online 15 July 2014

Editor: Carla M. Koretsky

Keywords:
Tufa
Fimmvörðuháls
Distribution coefficient
Coprecipitation
Rhombohedral
Immobilization

ABSTRACT

The reaction of CO_2 and water with basaltic rock can release trace heavy metals, which pose a serious threat to the quality of surface waters. The pH of the carbonated water increases during dissolution of the host rock or dilution by pore fluids. This leads to precipitation of carbonate and other secondary minerals that often scavenge the released heavy metals. However, very little is known about uptake capacity of the precipitates in natural systems or how much divergence there could be, compared with behavior in laboratory experiments. The spring 2010 eruption of the Eyjafjallajökull volcano, Iceland, provides a unique opportunity to study the mobility of heavy metals that are released during CO_2 injection into shallow basaltic aquifers and the ensuing precipitation of carbonate minerals.

Following the Eyjafjallajökull eruption, rapid and constant travertine formation was discovered in the Icelandic river, Hvanná, in the vicinity of the volcano. The river water emerged from under the lava flow and was heavily charged with cations and dissolved CO_2. The concentration of the major dissolved constituents was: dissolved inorganic carbon (DIC), 33.08 mM; calcium, 6.17 mM; magnesium, 4.27 mM; sodium, 2.78 mM and sulfur, 1.92 mM. Carbon dioxide degassing of the river water increased pH from 6.6 to 8.5 and travertine precipitated for hundreds of meters downstream, rendering the stream bed white with calcite. Rapid crystallization rate produced dendritic structures or sometimes very porous material. Boxwork textures were observed within the porous calcite that probably originated from transformation of a metastable phase such as ikaite ($CaCO_3 \cdot 6 H_2O$). A gradual decrease of conductivity from 1.8 mS/cm at the river water outlet to 1.1 mS/cm downstream and a clear drop in dissolved metal concentration strongly correlated with the precipitated calcite. Considering the complexity of the natural system, the estimated partition coefficients for Ba, Cd, Co, Cu, Mg, Mn, Na, Ni, Sr and Zn are in good agreement with the values derived from laboratory experiments under rather ideal conditions. Other elements were also scavenged from the river water, including Al, Fe, K, P, S, Si, Ti, V and the rare earth elements (REE). Our thermodynamic modeling suggests that, in addition to calcite and ikaite, silica, clay minerals, ferrihydrite, gibbsite and amorphous Ca, Mg carbonate minerals were supersaturated as the spring water degassed its CO_2. Our results provide a valuable base for assessing the environmental impact of volcanic eruptions in basaltic terrain and carbon capture and storage (CCS) in basaltic rock.

1. Introduction

The capture and storage of anthropogenic carbon dioxide in basaltic rock is a promising way of reducing CO_2 emissions (Seifritz, 1990; Bachu et al., 1994; Lackner et al., 1995; McGrail et al., 2006, 2011; Alfredsson et al., 2008, 2013; Goldberg et al., 2008; Oelkers et al., 2008; Gislason et al., 2010; Aradottir et al., 2012; Power et al., 2013; Gislason and Oelkers, 2014). Injection of CO_2 into rock formations in natural and engineered systems creates corrosive, CO_2 charged fluids with pH of 3 to 4 (Gislason et al., 2010; McGrail et al., 2011; Alfredsson et al., 2013). This occurs for example following an intrusion of magma at a shallow level in the crust, with the ensuing release of CO_2, or following the injection of CO_2-water mixtures for carbon capture and storage (CCS). These corrosive fluids dissolve the host rock and release the major cations, Ca^{2+}, Fe^{2+} and Mg^{2+}, but they can also mobilize toxic metals, especially in the early stages of water–rock interaction while the pH is still low (Aiuppa et al., 2000a,b, 2003, 2005; Rogers et al., 2006; Flaathen et al., 2009; Gislason et al., 2010; Alfredsson et al., 2013; Galeczka et al., 2013a,b; Olsson et al., 2013). Dissolution, especially of mafic rock, dilution by the original fluids in the pores and fissures of

* Corresponding author at: Room C112, Nano-Science Center, Department of Chemistry, University of Copenhagen, Universitetsparken 5, DK-2100 København Ø, Denmark. Tel.: +45 21 18 10 79; fax: +45 35 32 03 22.
E-mail addresses: jolsson@nano.ku.dk (J. Olsson), stipp@nano.ku.dk (S.L.S. Stipp), emilm@geo.ku.dk (E. Makovicky), sigrg@raunvis.hi.is (S.R. Gislason).

http://dx.doi.org/10.1016/j.chemgeo.2014.06.025
0009-2541/

the host rock and CO_2 degassing would raise pH and lead to precipitation of carbonate and other secondary minerals (Rogers et al., 2006; Kelemen and Matter, 2008; Flaathen et al., 2009; Olsson et al., 2012; Alfredsson et al., 2013; Bickle et al., 2013; Galeczka et al., 2014). The question remains, to what extent are the toxic metals sequestrated by precipitation in, or adsorption on secondary minerals? Uptake of trace metals would minimize pollution of ground and surface waters in volcanic terrain and in the vicinity of CO_2 injection wells in engineered systems.

After the 2010 eruption of the Eyjafjallajökull volcano in Iceland, travertines precipitated from the basic solutions that resulted from water percolation through the fresh basalt as CO_2 degassed from them. These travertines offer a unique opportunity to investigate the uptake of heavy metals that would likely result from CO_2 injection into shallow basaltic aquifers. Coprecipitation experiments conducted in laboratory settings provide data but it is quite possible that they do not reflect the true behavior of more complex, natural systems. The study of the natural travertine formation in the Hvanná River would give insight into how carbonate minerals take up heavy metals in the environment, which is certain to be closer to what would happen during carbon storage in basaltic rock.

After 18 years of deformation and earthquake activity, Eyjafjallajökull began an effusive flank eruption at the Fimmvörðuháls ridge on March 20, 2010 and it lasted until April 12 (Pedersen and Sigmundsson, 2004, 2006; Sigmundsson et al., 2010). An explosive summit eruption started on April 14, 2010 and ended in May 2012 (Fig. 1a). Eyjafjallajökull produces lava flows with basaltic to intermediate composition and the material from the 2010 eruption was relatively primitive and mildly alkaline basalt (Sigmarsson et al., 2011). Prior to eruption in the spring of 2010, the main riverine CO_2 flux from the volcano was via Gigjökull, the runoff stream from the caldera (Gislason et al., 1995). In July 2010, new measurements showed high concentrations of dissolved inorganic carbon in the river water of Hvanná. The CO_2 probably originated from a southeast tilted dyke intruded in March 2010 directly beneath the Hvanná valley, that did not reach the surface (Fig. 1a) (Sigmundsson et al., 2010). In the stream bed of the Hvanná, a layer of white travertine precipitated that was observed for the first time on April 2, 2010. At some places, it was already several centimeters thick in July 2010, covering rocks and twigs, and it extended for hundreds of meters downstream. The dissolved concentration of a wide range of elements decreased downstream, in parallel with the formation of the travertine so our hypothesis was that they were being taken up by the precipitating travertine.

The purpose of this study was to characterize the precipitated material by (1) identifying the phases, (2) characterizing the changes in crystal habit and morphology and (3) estimating the concentration of the scavenged elements. We have derived partition coefficients for the coprecipitated metals and compared their values with those from the literature. Our results provide a valuable base for assessing the environmental impact of volcanic eruptions and magma intrusion at shallow levels in the crust, as well as for carbon capture and storage (CCS) in basaltic rock, such as the Icelandic CarbFix project at the Hellisheiði injection site in Southwest Iceland and the Wallula project in Southeastern Washington.

2. Description of the field site and sample collection

2.1. Field site

A new spring outlet was observed emerging from under the lava flow of the Eyjafjallajökull 2010 flank eruption. The water had high

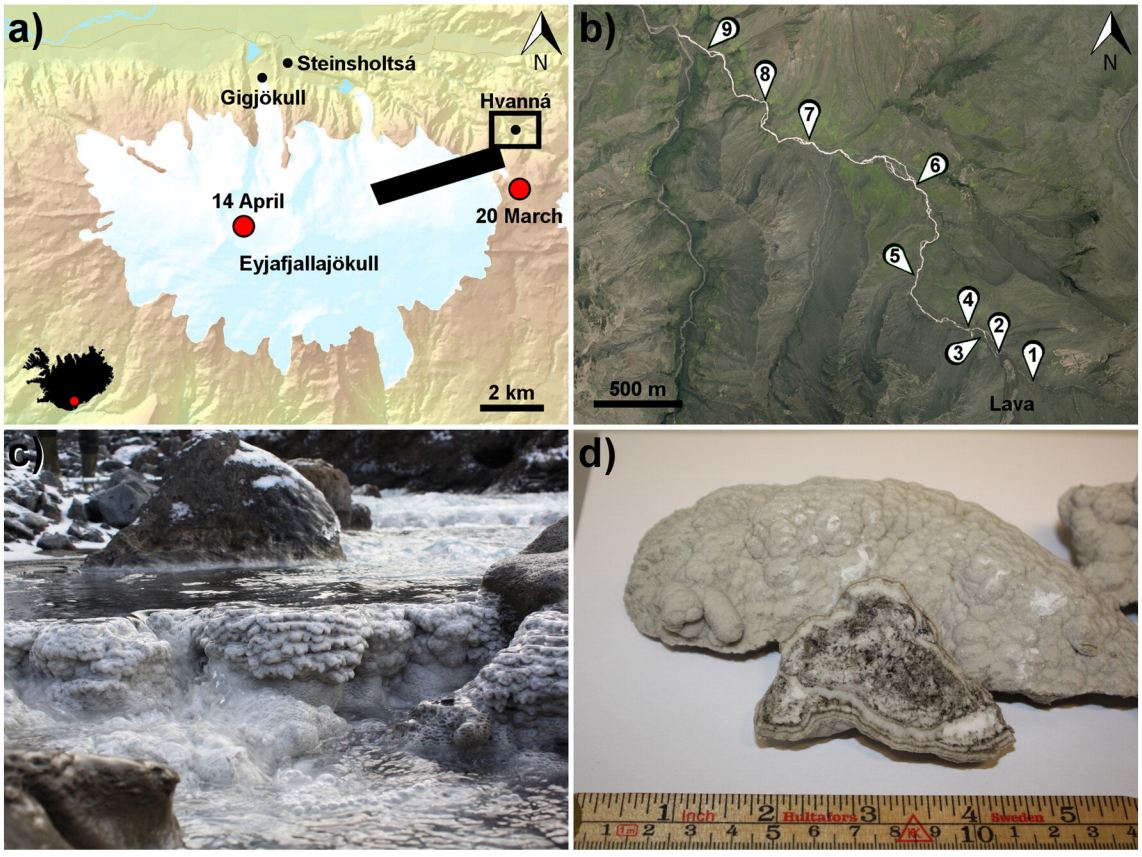

Fig. 1. Sample area and samples. (a) Map of the Eyjafjallajökull volcano. The red dots mark the eruption sites, the solid bar represents the area of an expected dyke intrusion based on deformation data (Sigmundsson et al., 2010) and the box outlined in black shows the sample area of (b), a modified satellite image from SAMSÝN, July, 2010 showing the sample locations; the white travertine shows as a heavy white demarcation of the Hvanná; (c) a photograph of sampling Site 6. (d) Travertine Sample HV03 from Site 6, showing the dark layers of altered ash that were captured as the travertine precipitated. (For interpretation of the references to color in this figure legend, the reader is referred to the web version of this article.)

concentrations of dissolved CO_2 and other constituents. About 100 m from the outlet, the river mixed with a very small, freshwater creek that runs through the Hvanná valley. Together they make the Hvanná River with a discharge of 0.44 m^3/s. We estimate that less than 5% of the Hvanná River originates in the freshwater creek. We found the first area of travertine in the riverbed just before the water from the lava flow mixed into the freshwater creek (Fig. 1b, Site 3). There was no travertine in the stream bed from where the waters merged into the river until about 750 m downstream. From there on, travertine was present and the amount increased with distance downstream toward Site 9. Travertine covered the entire stream bed and at some locations, the layer was several centimeters thick.

2.2. Sample collection and field measurements

We collected samples in the Hvanná valley on three occasions over four months. The first river water samples were collected July 8, 2010, less than 3 months after the flank eruption of Eyjafjallajökull had ended (March 20 to April 12, 2010). The second set of river water samples was collected on July 21, 2010. The last sample session was completed October 20–21, 2010, where both solid and river water samples were collected. This paper mainly discusses the last set of samples but all of the data from the previous campaigns are found in Table 1 and the Electronic Supplements ES-1.

In the field, we measured water temperature, electric conductivity and pH. The pH was measured using a plastic body, double junction electrode and the pH meter was calibrated against certified buffers from Oakton. The buffers were cooled to river temperature to minimize calibration errors. Samples for chemical analysis were filtered through 0.2 μm cellulose acetate membranes. We used acid rinsed plastic vials for sample collection, except for samples intended for anion analysis, which were collected in clean plastic vials. The vials were flushed with 3 rinses of the filtered water before the samples were collected. Samples intended for analysis by inductively coupled plasma optical emission spectrometry (ICP-OES) were acidified (1/90) with concentrated, suprapure HNO_3, on site. Vials with non-acidified samples developed a white precipitate within a couple of days. Samples for alkalinity titration were collected in preflushed, 2 l plastic containers, sealed and kept cold. Alkalinity was determined within 24 h of collection by Gran titration, using HCl (Gran, 1952; Stumm and Morgan, 1981). For determining dissolved oxygen concentration, river samples were collected in 50 ml Winkler bottles and the dissolved oxygen was stabilized as a precipitation of manganese hydroxide and titrated by the classical Winkler method (Winkler, 1888). The river discharge was determined by measuring cross sectional area and flow velocity. An overview of all samples, with collection dates, locations, water temperature, pH, electric conductivity, dissolved inorganic carbon (DIC) and oxygen concentration is given in Table 1.

3. Material and experimental methods

3.1. Flash dissolution experiments

The hand specimens of solid travertine samples contained small amounts of dark silicate mineral particles cemented within, as shown in Fig. 1c and d. This material was identified with X-ray diffraction (XRD) and energy dispersive X-ray spectroscopy (EDXS) as Eyjafjallajökull ash. To minimize element contributions from the ash, only the travertine from the surface of the samples was used. It was crushed in an agate mortar and 0.1 g was dissolved in 10 mL of a 1% HNO_3 solution, pH 0.8, in a plastic syringe for 1 min. It is known that calcite dissolves at least 5 orders of magnitude faster than basaltic glass, crystalline basalt, quartz and clay minerals (Chou and Wollast, 1985; Busenberg and Plummer, 1986; Brady and Walther, 1990; Pokrovsky and Schott, 2000; Gislason and Oelkers, 2003, 2011; Köhler et al., 2003) so we could assume that contribution from phases other than calcite was minimal. After dissolution, each solution was filtered through 0.2 μm cellulose acetate membrane filters into acid washed, polypropylene bottles. The samples were analyzed at Analytica-SGAB, Luleå, Sweden, with ICP-OES, inductively coupled plasma sector field mass spectroscopy (ICP-SFMS). Hg was measured with atomic fluorescence spectroscopy (AFS). The results were used to derive the trace element concentrations in the travertine. All concentrations and uncertainties are reported in the electronic supplement, ES-2. We also derived concentrations using quantitative chemical microprobe analysis. These results had an analytical error of approximately 0.01 wt.%. The two methods gave the same results, within uncertainty limits. The measured metal concentrations were normalized to 1 mol of dissolved calcite, assuming all Ca ions originated from pure calcite.

3.2. Characterization techniques and parameters

The mineral composition of the travertine was determined by standard X-ray diffraction (XRD) with a Bruker D8 Advance X-ray Diffractometer equipped with a Cu-Kα radiation source. The pure calcite used as an XRD reference in Fig. 2 was commercial, reagent grade calcite purchased from Sigma. Polished thin sections of the travertine samples were examined with polarized light microscopy in a Zeiss AXIO Imager A1m Laboratory Microscope. For quantitative chemical microprobe analysis, the polished thin sections were coated with 10 nm of carbon and then examined with a JEOL microprobe (JXA-8200) operated at an accelerating voltage of 15 kV, beam current of 8 nA and spot size of 10 μm. For standards, we used natural and

Table 1
Overview of the sampling sites along the river Hvanná. About 25% more water had accumulated in the discharge of the river at Site 8 from small tributaries. The H_2S concentration was <0.2 μM at the river outlet from under the lava flow. E_c represents the electric conductivity and DIC, the dissolved inorganic carbon.

Site #	River sample	Travertine sample	Sampling date (YYMMDD)	Location (latitude and longitude)		Distance from the outlet (m)	Water temp (°C)	pH	E_c (μS/cm)	DIC (mM)	Oxygen (mM)	Discharge (m^3/s)
1	10EF75	NA	101020	63°39.056′	019°26.725′	−100	1.6	8.5	87.6	NA	0.35	NA
2	10EF72	NA	101020	63°39.103′	019°26.843′	0	4.8	6.6	1805	33.08	0.09	NA
3	10EF76	HV01	101020	63°39.129′	019°26.898′	100	4.6	7.5	1744	NA	NA	NA
4	10EF74	NA	101021	63°39.142′	019°26.953′	220	4.4	7.2	1848	26.06	0.29	0.44
5	10EF79	HV02	101021	63°39.231′	019°27.152′	780	4.2	8.1	1781	NA	NA	NA
6	10EF80	HV03	101021	63°39.380′	019°27.163′	1300	5.5	8.4	1338	NA	NA	NA
7	10EF81	HV04	101021	63°39.453′	019°27.559′	2170	5.3	8.5	1171	NA	NA	NA
8	10EF82	HV05	101021	63°39.517′	019°27.718′	2385	5.4	8.5	1035	NA	NA	NA
9	10EF73	HV06	101021	63°39.599′	019°27.954′	3100	5.2	8.5	1107	9.13	0.32	NA
4	10EF68	NA	100708	63°39,142′	019°26,953′	220	3.5	7.2	1652	28.20	NA	0.47
4	10EF69	NA	100721	63°39,142′	019°26,953′	220	3.3	7.2	1732	28.42	NA	0.39
5	10EF70	NA	100721	63°39,231′	019°27,152′	780	3.9	8.0	1726	21.93	NA	NA

NA, not available; BDL, below detection limit.

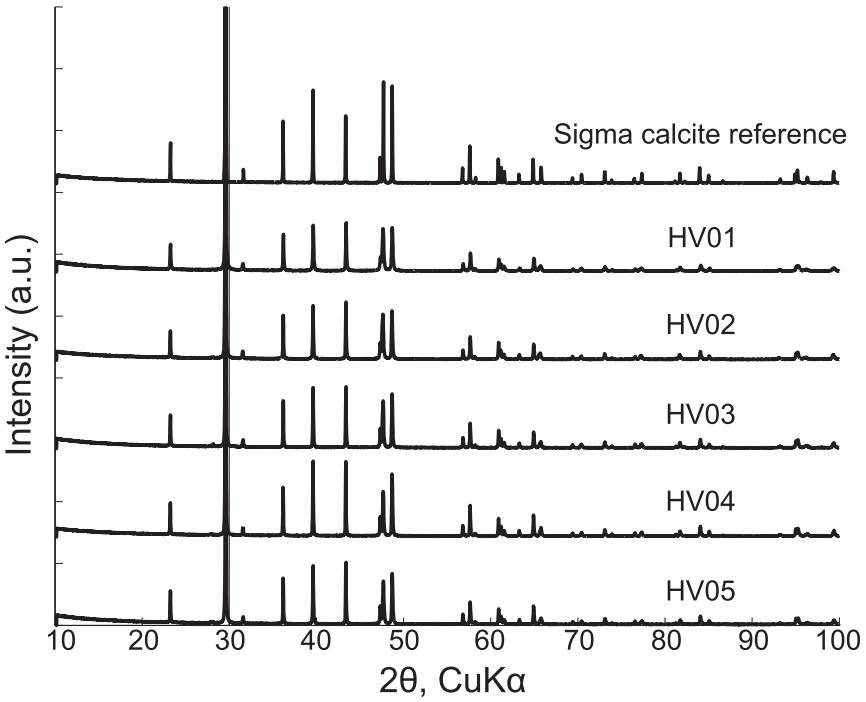

Fig. 2. X-ray diffraction patterns from five samples from along the Hvanná flow path and synthetic calcite for reference. Calcite is the only crystalline phase observed. The differences in peak intensity are ascribed to preferred orientation of the rhombohedral crystals.

synthetic silicates and oxides. The counting time was 20 s, except for Fe, where it was 40 s. Scanning electron microscopy (SEM) images were collected with a FEI Quanta 3D SEM, with energy dispersive X-ray spectroscopy (EDXS).

The chemical components of the river samples and the flash dissolved samples were analyzed with ion chromatography (IC) and inductively coupled plasma optical emission spectrometry (ICP-OES) at the Institute of Earth Sciences, University of Iceland, and standardized with inhouse multi element standards, verified against the SPEX certified reference standards. Selected samples were analyzed at Analytica-SGAB, Luleå in Sweden, with ICP-OES, inductively coupled plasma sector field mass spectroscopy (ICP-SFMS) and Hg was measured with atomic fluorescence spectroscopy (AFS). The differences in the concentrations measured in house and at Analytica-SGAB were within the limits of uncertainty. Forty two elements were analyzed, including the rare earth elements (REE). A full list of the concentrations and uncertainties of all elements can be found in Table 2 and the Electronic Supplements ES-2.

The geochemical computer modeling program PHREEQC, with the PHREEQC database, was used to determine the charge balance and the saturation states (Parkhurst and Appelo, 1999). PHREEQC is a powerful aqueous speciation program designed for geochemical modeling. In combination with thermodynamic data from the literature and various other databases, we used PHREEQC in this work to estimate saturation state of a large range of mineral phases. Additional thermodynamic data were added for ikaite (Bischoff et al., 1993a), allophane and imogolite (Stefansson and Gislason, 2001). Additional modeling was made using the MINTEQ.v4 database to identify the saturation state of nesquehonite, hydromagnesite, magnesite and dolomite.

4. Calculations

The partition coefficient expresses the ability of a particular phase to scavenge a foreign element. The phase in this study is calcite and the foreign element is any metal ion (Me). The partition coefficient is defined as:

$$p_{Me} = \frac{X_{Me,s}}{X_{Ca,s}} / \frac{c_{Me,l}}{c_{Ca,l}}, \quad (1)$$

where $X_{Me,s}$ and $X_{Ca,s}$ represent the mole fraction of the scavenged metal and Ca in the solid phase and $c_{Me,l}$ and $c_{Ca,l}$ represent the molar concentration of the metal and Ca in the river water. The partition coefficient is determined empirically and should not be confused with the thermodynamically defined distribution coefficient, often labeled K_D or D (Morse and Bender, 1990; Stumm, 1992). When p_{Me} is above unity, the corresponding metal is scavenged by the precipitating calcite, decreasing the dissolved Me/Ca ratio. For p_{Me} below unity, the metal ion is incorporated into calcite to a lower extent than Ca, so the solute Me/Ca ratio increases. A number of physicochemical factors can impact the partition coefficient for some metals. These include pH, stirring rate, temperature, pressure, ionic strength, oxidation level, precipitation rate and composition of the parent solution (Kitano et al., 1980; Morse and Bender, 1990; Stumm, 1992; Rimstidt et al., 1998; Curti, 1999).

5. Results

5.1. The chemistry of the Hvanná River

On 8 July 2010, only a few months after the eruption of the Eyjafjallajökull volcano, a new, strong output of riverine CO_2 was observed passing through the river Hvanná. Increased partial pressures of CO_2 were detected with a simple gas monitor in the air above the water surface. The DIC concentration was 33.08 mM in the springs feeding the river (Site 2) and it decreased to 9.13 mM at Site 9, 3 km downstream (Table 1). For comparison, in other rivers that carry the runoff water from the main glacier covering the north site of the volcano, DIC varied from 0.47 mM for Steinsholtsá to 2.87 mM for Gigjökull (Fig. 1a and Electronic Supplements ES-1). The pH increased from 6.6 at the spring to

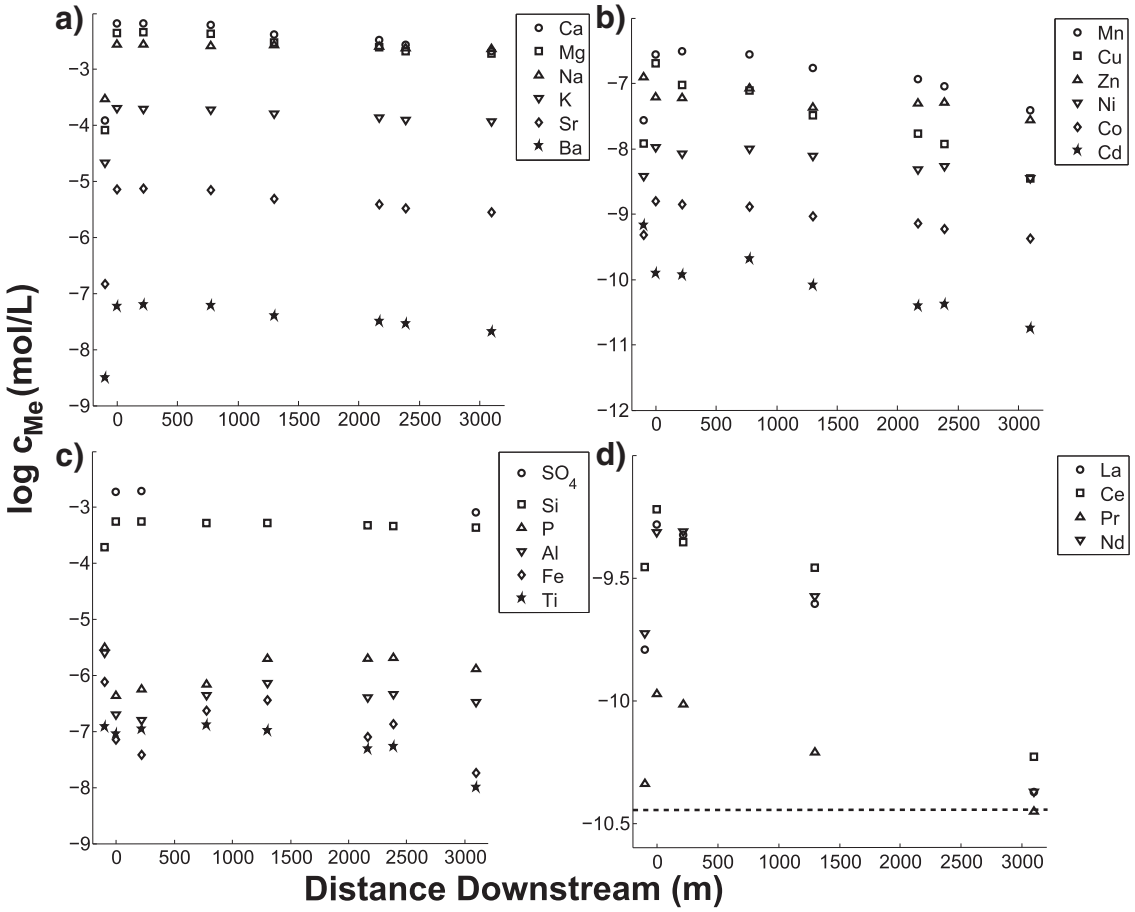

Fig. 3. Element concentrations measured with distance downstream along the Hvanná River: a) alkali and alkaline earth metals; b) transition elements of divalent cations; c) other ions of interest; and d) the rare earth elements. Most species decreased continuously with distance downstream. The concentration of Si decreased slightly while Al, Fe, Ti and P changed discontinuously. Most of the uncertainties are within the dimension of the symbols. A full list of measured concentrations and estimated uncertainties is presented in Table 2. The dotted line represents the detection limit. The average water velocity was 0.8 m/s so water sampled at Site 1 reached Site 9 about 1.1 h later.

8.5 at Site 9; electrical conductivity decreased from 1810 to 1110 μS/cm. Dissolved oxygen increased almost instantly from 0.09 mM in the spring water to 0.29 mM, which is close to equilibrium with air. The average velocity of the water was 0.8 m/s so the water that flowed out of the spring at Site 2 ran 3100 m to Site 9 in ~1.1 h.

River discharge at Site 4 was 0.44 m^3/s in October 2010. Estimated from the water influx from the smaller creeks, the river discharge increased by ~50% by the time it reached Site 9. This corresponds to a dilution of ~30% over the entire flow path. The concentration for most of the dissolved elements decreased with distance downstream at a rate much higher than could be explained by dilution. Calcium decreased continuously along the flow path, by a total of 69%, from 6.69 to 2.07 mM (Table 2). The other divalent cations followed a similar trend, all decreasing by more than 30%. In order, these are: Cu, 96%; Mn, 87%; Cd, >85%; Co, 71%; Ba, 67%; Sr, 63%; Ni, 59%; Mg, 58% and Zn, 55% (Fig. 3a and b). The concentration of Na and K decreased by 16% and 41%, and silicon decreased by 22%, from 0.50 to 0.39 mM (Table 2). The concentrations of Al, Fe, Ti and P changed discontinuously (Fig. 3c). The concentrations of Al, Cd, Fe, P, Ti and Zn in water that emerged from under the lava flow at Site 2 were lower than water from the freshwater creek at Site 1, above the lava flow (Fig. 1b). Of the rare earth elements (REE), only concentrations of Ce, La, Nd and Pr were above the detection limit and these decreased rapidly downstream (Fig. 3d and Table 2). The concentration of other REE, including Dy, Er, Gd, Sm and Yb, followed a similar trend but these were at the limit of detection. Fluoride concentration was low but increased from 0.0012 to 0.014 mM along the flowpath, Cl^- decreased by 34%, from 0.50 to 0.33 mM, whereas the concentration of SO_4^{2-} was initially high and decreased from 1.97 to 0.81 mM, 59% (Table 2).

An easy way to correlate the change in metal concentration in the Hvanná River with the precipitated calcite is to plot the dissolved metal to the calcium concentration and derive R^2 for a simple linear regression. Several elements showed high correlation, including Sr, Mn, Mg, Ba, Co and Cu (Table 3). Other elements with lower correlation are Si, Ni, Ti, Cd, Na, Zn and P, whereas Al and Fe showed no correlation. The concentrations of Al, Fe, P, and Ti were poorly correlated with each other and to other elements.

5.2. Characterization of the travertine deposits

Six solid travertine samples were collected along the flow path of the Hvanná River. They were white to gray and their texture was uneven, resembling the surface of cauliflower. When fractured, all samples except one had distinct layers of darker material (Fig. 1d). Energy dispersive X-ray spectroscopy (EDXS) revealed that these layers were Si rich, with increased levels of Al and Na and an X-ray diffraction (XRD) analysis suggested phases of plagioclase and pyroxene together with amorphous or nanocrystalline material. This matches the composition of the Eyjafjallajökull ash (Gislason et al., 2011). The far more dominating white to gray travertine was separately examined to identify primary and secondary phases and to gain information about crystal structure.

From XRD, we could identify only calcite in all analyzed samples (Fig. 2); no vaterite, aragonite or ikaite were visible. Mismatch of sample

Table 3
Summary of the data used to show the correlation between the dissolved metal and calcium concentrations, the partition coefficients (p_{Me}) determined with Eq. (1) for the travertine and the range of metal concentrations measured in the Hvanná River. For comparison, partition coefficients reported in the literature for experiments in ideal systems are listed (data from compilations by Rimstidt et al. (1998) and Curti (1999)). Metals with low correlation are not expected to be taken up by calcite. REE concentration in the river water for La, Ce, Pr, Nd, Sm, Gd, Dy, Er and Yb decreased along the flow path but concentrations were too close to the detection limit, thus uncertainties were too high, to determine if there was a correlation with Ca and p_{Me}.

Measured values					Literature data				
Metal	Linear corr. of Me(aq) to Ca(aq) (R^2)	Number of p_{me} values	Metal conc. in river water(mM)	Partition coefficient (p_{me}) range	Partition coefficient (p_{me}) range	Metal conc. (mM)	pH	Temp. (°C)	Reference
Sr	0.9982	6	$2.8\cdot10^{-3}$–$8.3\cdot10^{-3}$	0.26–0.37	0.15–0.40	0.09	7.7–8.0	25	Mucci and Morse(1983)
Mn	0.9967	6	$3.9\cdot10^{-5}$–$3.5\cdot10^{-4}$	3.4–13.1	3.1–12.2	1	5.5–6.7	10	Dromgoole and Walter(1990)
Mg	0.9957	6	1.9–5.1	0.012–0.018	0.010–0.032	80–110	7.7–8.2	25	Mucci and Morse(1983)
Ba	0.995	6	$2.0\cdot10^{-5}$–$7.1\cdot10^{-5}$	0.63–1.2	0.04–0.12	0.02–0.04	n.a.	25	Pingitore and Eastman(1984)
Co	0.9942	6	$4.2\cdot10^{-7}$–$1.9\cdot10^{-6}$	1.4–2.8	1.9–5.9	$8.5\cdot10^{-6}$	7.3–7.5	25	Lorens(1981)
Cu	0.9788	6	$3.5\cdot10^{-6}$–$1.4\cdot10^{-4}$	7.8–50	23.3–25	$3.2\cdot10^{-3}$–$6.3\cdot10^{-3}$	n.a.	25	Kitano et al.(1980)
Ni	0.8498	6	$3.5\cdot10^{-6}$–$9.9\cdot10^{-6}$	0.15–0.44	~1	0.01–0.06	8.3–8.4	25	Lakshtanov and Stipp(2007)
Ti	0.8231	6	$9.7\cdot10^{-6}$–$1.3\cdot10^{-4}$	1.9–11					
Cd	0.7732	5	$3.9\cdot10^{-8}$–$2.0\cdot10^{-7}$	4.5–51	9.1–66.1	$2\cdot10^{-7}$	7.3–7.6	25	Lorens(1981)
Na	0.6712	6	2.3–3.0	$6.9\cdot10^{-4}$–0.0040	0.001–0.006	5–30	6.1–8.3	25	Okumura and Kitano(1986)
Zn	0.6574	6	$2.7\cdot10^{-5}$–$8.4\cdot10^{-5}$	0.90–16	25–27	0.01	7.0–8.5	25	Kitano et al.(1980)
Al	0.0692	6	$2.0\cdot10^{-4}$–$7.2\cdot10^{-4}$	1.0–12.4					
Fe	0.0408	6	$1.8\cdot10^{-5}$–$3.6\cdot10^{-4}$	0.93–50	1.5–2.3	0.1	5.5–6.7	10	Dromgoole and Walter(1990)

NA, not available.

peak intensities compared with the reference sample resulted from preferred orientation with $\{10\bar{1}4\}$ faces lying on the flat sample holder.

The SEM showed very porous material without a well defined crystal habit but a minority of particles was recognizable rhombohedra (Fig. 4). In the polished thin sections, using polarized light microscopy, the very porous nature of the travertine was clear, with crystals growing as dendrites perpendicular to the substrate (Fig. 5a). Each of the dendrites consisted of several branches radiating from a central axis. Parallel extinction of the dendrites indicates growth along the *c*-axis and parallel extinction of branches from a shared central axis suggests calcite twinning. Continuous layers of Si rich material were visible between the calcite dendrites (Fig. 5b). The section from sample HV03 showed straight and curved lines that divide aggregates of fine grained calcite into boxes or compartments (Fig. 5c). The chemical composition of the dendritic calcite and the porous compartments was determined

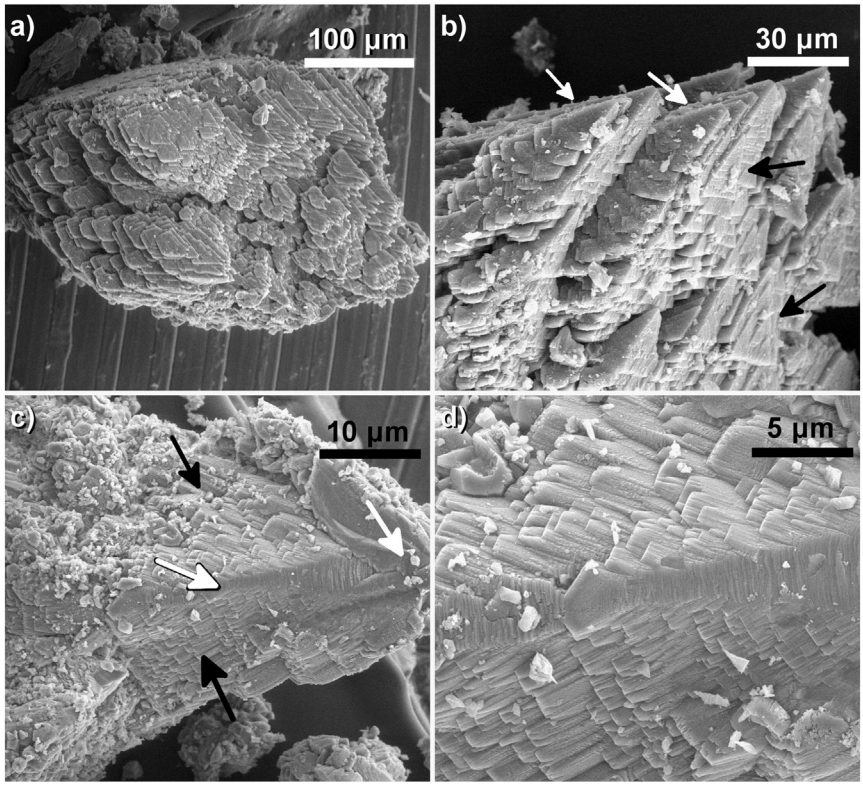

Fig. 4. SEM pictures of calcite deposits: a and b) from sample HV01 and c and d) from HV05. a) "loose" calcite. The crystal growth direction was limited by the supply of Ca^{2+} and CO_3^{2-} and competition by the neighboring crystals. Mass flux and fast crystallization resulted in porous aggregates, dominated by dendritic growth. b) Calcite grown as a series of intersecting rhombs with the *c*-axis toward the upper right corner of the image. Close to perfect $\{10\bar{1}1\}$ faces are visible on the right side (black arrows) and the faces on the left were overgrown by the $\{10\bar{1}4\}$ form (white arrows), probably during the last stage of crystallization. c and d) show an elongated calcite crystal, interpreted as the $\{10\bar{1}1\}$ form, overgrown by imperfect $\{10\bar{1}4\}$ forms. The tip and edges are protruding (white arrows) relative to the recessed crystal faces (black arrows).

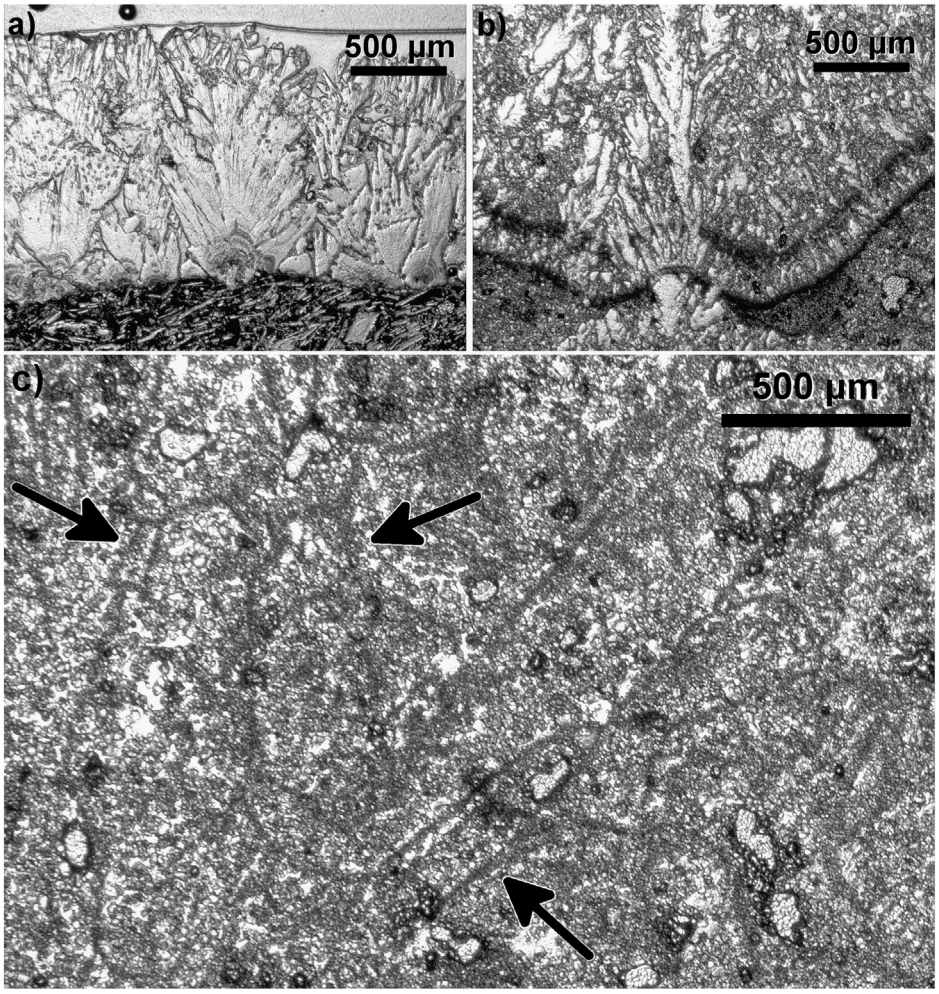

Fig. 5. Light microscopy photos of selected areas on Sample a) HV01 and b and c) HV03. a) Several dendrites that grew out from their nucleation sites on the underlying substrate. b) Selected calcite grains that penetrate layers of cemented ash. c) Old crystal boundaries (black arrows), that were probably edges of the metastable hydrated $CaCO_3$ phase called ikaite, that transformed into fine grained calcite.

with microprobe analyses. The composition was similar but the compartments contained slightly more Si and marginally less Mg, S and Sr (Table 4). The chemical composition of the calcite in the travertine samples was measured by a second method, i.e. flash dissolution of the travertine samples and then the components that were released to the solution were analyzed (as described in Section 3.1). The average concentration of the detected elements per mole of calcite can be found in Table 5.

Table 4
Chemical composition of three selected travertine samples. Samples HV01, HV03 and HV05 were analyzed with an electron microprobe. The values listed are averages of at least seven measurements from various areas of the samples. The data for HV03 are from the dendritic calcite and the calcite within compartments seen in Fig. 5c.

Oxide wt%	HV01, dendritic calcite	HV03, dendritic calcite[a]	HV03, calcite compartments[a]	HV05, dendritic calcite
SiO_2	0.00	0.00	0.09	0.01
FeO	0.09	0.01	0.01	0.00
CaO	54.72	55.36	55.68	55.34
MgO	0.33	0.35	0.27	0.36
Na_2O	0.04	0.04	0.04	0.05
MnO	0.03	0.03	0.01	0.02
SrO	0.05	0.06	0.03	0.04
SO_3	1.04	0.84	0.80	0.47
CO_2	42.95	43.44	43.7	43.43
Total	99.26	100.1	100.6	99.72

[a] Extra analyses showed Al_2O_3, BaO, Cl, F and TiO_2 to be all below the detection limit.

6. Discussion

6.1. Morphology of the calcite

Loose aggregates, very porous material and dendritic precipitation are expected for very fast crystallization or precipitation from solutions that are highly supersaturated (Meakin and Jamtveit, 2010). The growing calcite crystals compete for space and for Ca^{2+} and CO_3^{2-} ions from solution so growth is favored perpendicular to the nucleation substrate. Rhombohedral crystals are the most stable form for calcite but in the travertine, the rhombohedra are often imperfect and overgrown by other crystal faces. For example, the SEM images in Fig. 4b show the rare $\{10\bar{1}1\}$ form; nearly perfect faces are visible on the right side of the grain, while on the left side is a different morphology, sculpted by the common $\{10\bar{1}4\}$ form. Fig. 4c and d shows another calcite crystal with $\{10\bar{1}1\}$ form but with a different face texture, possibly modified by the forms $\{10\bar{1}2\}$ or $\{10\bar{1}4\}$. An interesting phenomenon is the recessed crystal faces and the raised tips and edges because this elongated crystal probably formed from supersaturated solution.

Precipitation on elevated areas, such as edges and tips, was favored, and they grew faster into the fluid, depleting local ion concentration, while the crystal faces were starved for Ca^{2+} and CO_3^{2-}.

The layered Si rich phases between the calcite dendrites (Figs. 1d and 5b) was river suspended ash from the Eyjafjallajökull eruption that was blown into the river and cemented by the precipitating travertine. If only a thin layer of ash adhered to the travertine surface, the dendrites could continue to grow through the layer, perhaps slightly disorientated or in crystallographic continuity. Thicker layers of ash completely block further growth of the dendrites but new crystals could nucleate and grow from the ash layer. A similar process has been observed in karst caves where layers of smectite form, slowing crystal growth and decreasing grain size in the radial calcite that forms in stalactite and stalagmite aggregates.

6.2. Calcite recrystallization from ikaite

The division of fine grained aggregate into compartments (Fig. 5c) is not typical for calcite. The box work texture of this aggregate probably arose from transformation of a metastable phase. We propose that calcite cemented the compartment boundaries and these persisted while the original crystals dissolved and were replaced by calcite at a later stage. It is possible that these original crystals were the hydrated form of calcium carbonate called ikaite ($CaCO_3 \cdot 6\ H_2O$), which forms at near freezing conditions and converts to vaterite or calcite at higher temperatures (Pauly, 1963; Suess et al., 1982; Shearman and Smith, 1985; Shearman et al., 1989). Subzero temperatures are common in the Hvanná area in the spring. Some ions such as Mg^{2+}, SO_4^{2-} and PO_4^{3-} particularly inhibit crystallization of the anhydrous $CaCO_3$ polymorphs and thereby indirectly promote ikaite precipitation (Shearman and Smith, 1985; Bischoff et al., 1993a; Council and Bennett, 1993; Larsen, 1994; Loste et al., 2003). Formation and subsequent decomposition of ikaite can explain the granular character of the calcite and the relic box work texture. The product of dehydrated and transformed ikaite would be highly porous calcite (Shearman and Smith, 1985; Shearman et al., 1989; Larsen, 1994). Natural precipitation of ikaite has only rarely been observed in nonmarine environments such as lake waters (Bischoff et al., 1993b; Council and Bennett, 1993) and cold saline spring waters (Ito, 1996; Omelon et al., 2001).

6.3. Prediction of stable mineral phases in Hvanná with PHREEQC

The saturation state of a large range of mineral phases in aqueous solutions can be tested using PHREEQC. We based our calculations on the sample collected at Site 2 (Fig. 1b), before precipitation began (data in Tables 1 and 2). The charge balance estimated from the analyses

Table 5
The average concentration of the detected ions per mole of calcite. The concentrations were derived from electron microprobe analyses and flash dissolution of the travertine samples following analyses of the chemical components released to solution, using ICP-SFMS and ICP-OES. The concentrations represent only the white travertine from the surface of the samples and not the granular calcite compartments (Section 6.2) or the ash located deeper within the samples.

Element	mmol/mol of calcite	Element	mmol/mol of calcite	Element	mmol/mol of calcite
S	9.9	Ti	0.074	Sm	$0.38 \cdot 10^{-3}$
Mg	9.5	Zn	0.043	Ni	$0.36 \cdot 10^{-3}$
Na	1.2	Ba	$8.8 \cdot 10^{-3}$	Er	$0.32 \cdot 10^{-3}$
P	1.1	La	$2.0 \cdot 10^{-3}$	Yb	$0.26 \cdot 10^{-3}$
Sr	0.43	Ce	$2.0 \cdot 10^{-3}$	Cd	$0.24 \cdot 10^{-3}$
Mn	0.3	Nd	$1.9 \cdot 10^{-3}$	Eu	$0.12 \cdot 10^{-3}$
Al	0.26	V	$0.96 \cdot 10^{-3}$	Ho	$0.11 \cdot 10^{-3}$
Cu	0.23	Gd	$0.51 \cdot 10^{-3}$	Tb	$0.07 \cdot 10^{-3}$
K	0.18	Dy	$0.46 \cdot 10^{-3}$	Lu	$0.04 \cdot 10^{-3}$
Fe	0.16	Co	$0.42 \cdot 10^{-3}$	Tm	$0.04 \cdot 10^{-3}$
Si	0.07	Pr	$0.41 \cdot 10^{-3}$		

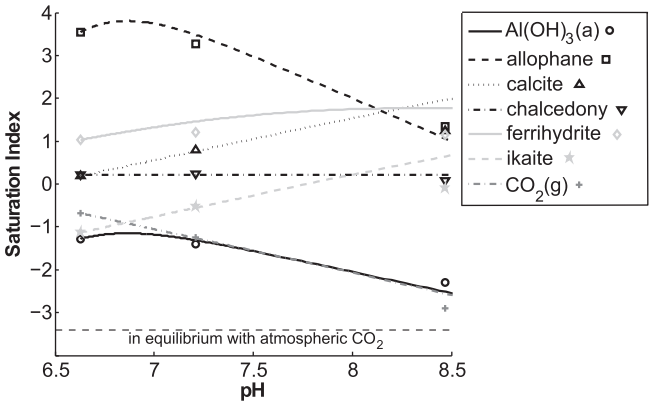

Fig. 6. The saturation state of selected minerals with respect to the river water at Sites 2, 4 and 9 are marked by the various symbols. The pH of the headwater before degassing at Site 2 is 6.6 but the highest is 8.5, at the end of the travertine deposits at Site 9, after significant degassing and carbonate mineral precipitation. The lines and curves depict the saturation state calculated by continuous degassing at Site 2, assuming no precipitation of secondary minerals. The dissolved CO_2 gas is at equilibrium with atmospheric CO_2 when the log of the partial pressure is −3.4, shown by the dotted horizontal line.

was good, −1.4%. The pH of the river water at this stage was 6.6, temperature 4.8 °C and partial pressure of the CO_2, log pCO_2, was −0.5 (Fig. 6), which was significantly higher than in air, where log $pCO_2 = -3.4$. The CO_2 therefore degassed, which was confirmed with direct measurements of the air above the stream at Site 2. Calcite precipitation from Ca and CO_2 rich waters, driven by degassing, is a common phenomenon (Dreybrodt et al., 1992; Lu et al., 2000; Hammer et al., 2005, 2007; Jamtveit et al., 2006). The water did not "bubble," because the partial pressure of CO_2 was <1 bar. Data from the river water sampled at Site 2, including temperature, composition, initial pH and alkalinity, were modeled where CO_2 was released in small steps until a pH of 8.5 was reached, such as at Sites 6, 7, 8 and 9 (Table 1 and Fig. 1b). This mimics CO_2 degassing and allows the solution to get closer to equilibrium with atmospheric CO_2. At pH 8.5, the modeled pCO_2 was −2.59, which still corresponds to a higher partial pressure than that of the atmosphere. The saturation state with respect to a set of selected minerals was determined at each degassing step but no minerals were allowed to precipitate.

The saturation indices are plotted against in situ pH in Fig. 6 for both the modeled CO_2 degassing (lines and curves) and the data estimated from samples from Sites, 2, 4 and 9 (data points). The phases that we estimate to be supersaturated, likely forming precipitates (Anthony et al., 2013) or present as weathering products (Stefansson and Gislason, 2001) were: calcite ($CaCO_3$), chalcedony (SiO_2), clay minerals (including allophane ($Al_2O_3(SiO_2)1.3 \cdot 2.5\ H_2O$) and imogolite ($Al_2SiO_3(OH)_4$)), poorly crystalline ferrihydrite (~$Fe(OH)_3$), gibbsite (α-$Al(OH)_3$), goethite (FeOOH) and ikaite ($CaCO_3 \cdot 6\ H_2O$). Several other phases were supersaturated but less likely to form. In order of decreasing supersaturation, these are: hematite (Fe_2O_3), hydroxylapatite ($Ca_5(PO_4)_3OH$), hausmannite (Mn_3O_4), dolomite ($CaMg(CO_3)_2$), manganite (MnOOH) and aragonite ($CaCO_3$). In Fig. 6, $Al(OH)_3$(a), allophane, chalcedony and ferrihydrite represent the formation products of the aluminum hydroxides, the clay minerals, silica and iron (hydr)oxides.

As expected, the saturation indices of the carbonates, calcite and ikaite, predicted for CO_2 degassing increased downstream. It is somewhat exaggerated because our model did not take precipitation or dilution effects into account. The saturation state calculated from the measured water composition at Site 9 is much lower than predicted from simple degassing of Site 2 waters because of considerable carbonate precipitation along the flow path, as shown in Fig. 6, and because of the dilution of the river water. Ferrihydrite shows a similar trend, which suggests some precipitation of this phase. The modeled saturation state of allophane and amorphous $Al(OH)_3$ at Site 9 however, is lower than

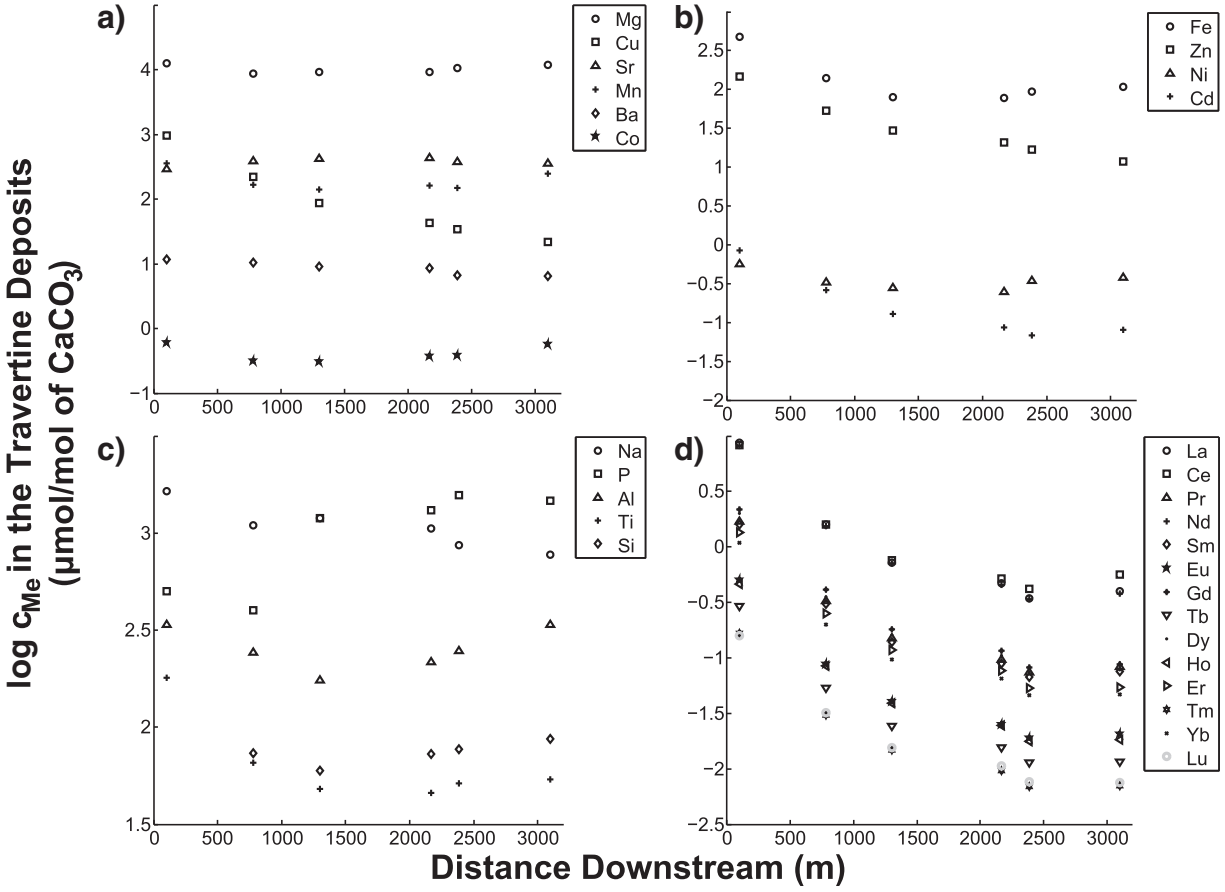

Fig. 7. The element concentration per mole of dissolved travertine as a function of distance downstream. The elements plotted were: divalent ions (a) with high and (b) low linear correlations with the dissolved Ca concentration; c) other ions d) and the REE. Analytical uncertainty is within the dimension of the symbols in most cases. The full data set of measured concentrations and estimated uncertainties is presented in the electronic supplements, ES-2.

the saturation state calculated from the measured water at Site 9, suggesting some addition of dissolved Al along the flowpath. This is in concert with the results shown in Fig. 3. The modeled and calculated saturation state of chalcedony along the flowpath and at Sites 4 and 9 are nearly identical suggesting no major precipitation and/or dissolution of silica containing mineral or glass.

At neutral pH, the river water of Hvanná was mostly supersaturated with respect to clay minerals and at more basic conditions, calcite was the dominant phase. Calcium carbonate and elevated levels of CO_2 promote the precipitation of silica (Lovering and Patten, 1962) but neither silica nor clays were expected to have precipitated directly in Hvanná. Silica is known to have an extremely slow polymerization rate (Alexander et al., 1954; Krauskopf, 1956) and clay minerals form very slowly at low temperature (Kerr, 1952; Carrado et al., 2006). Silica and clays, along with aluminum and iron hydroxides, could only have formed as alteration products of basaltic to andesitic material, e.g. the windblown ash (Stefansson and Gislason, 2001). The amount of silica phases formed in the river channel is negligible, because the concentration in the downstream samples has not changed much beyond what could be accounted for by dilution (described in Section 5.1). Furthermore, small amounts of dissolved Si can be incorporated by calcium carbonate (Kitano et al., 1979; Klein and Walter, 1995; Belova et al., 2013). Despite the low iron concentration, ferrihydrite is likely to have formed. It is a precursor for both goethite and hematite (Schwertmann and Cornell, 2000). Usually, calcite was the most supersaturated phase for the solid samples collected at pH > 8 but ikaite was also supersaturated at higher pH. Inhibition of calcite precipitation by Mg^{2+}, SO_4^{2-} and PO_4^{3-} was not considered in the model but these ions would favor ikaite precipitation especially where river temperature is low.

6.4. Coprecipitation of the dissolved elements in the river water of Hvanná

Formation of ferrihydrite, other alteration products of river suspended ash or of significant amounts of hydrated carbonates, e.g. ikaite and amorphous Ca, Mg carbonates (Radha et al., 2012) could influence water composition by taking up a fraction of the dissolved constituents. However, Ca concentration is about five orders of magnitude greater than Fe (Fig. 3) and there is a clear decrease in Ca concentration downstream but Fe does not decrease (Fig. 3). This is logical because in these oxidizing waters, Fe^{2+} activity would be very low. Calcite was by far the main precipitate in Hvanná and was the only crystalline phase detected in our travertine samples. Thus, we assume that calcite is the dominant scavenger of trace elements from the Hvanná River. A large number of minor and trace elements can be sequestered by calcite in several ways. They can be adsorbed as a result of electrostatic interactions, physically trapped between crystal planes. They can occupy vacant structure position caused by crystal defects or substitute directly for Ca^{2+} or CO_3^{2-} in the crystal structure. The amount and type of foreign constituents taken up by calcite depends on ionic radius and charge relative to Ca^{+2} or CO_3^{2-} and on their availability in the river water. The amount of foreign ions incorporated into calcite is positively correlated with growth rate because of a larger incidence of crystal defects and less time to reach equilibrium (Pentecost, 2005). For example, Busenberg and Plummer (1985) found higher SO_4^{2-} uptake in calcite grown at higher precipitation

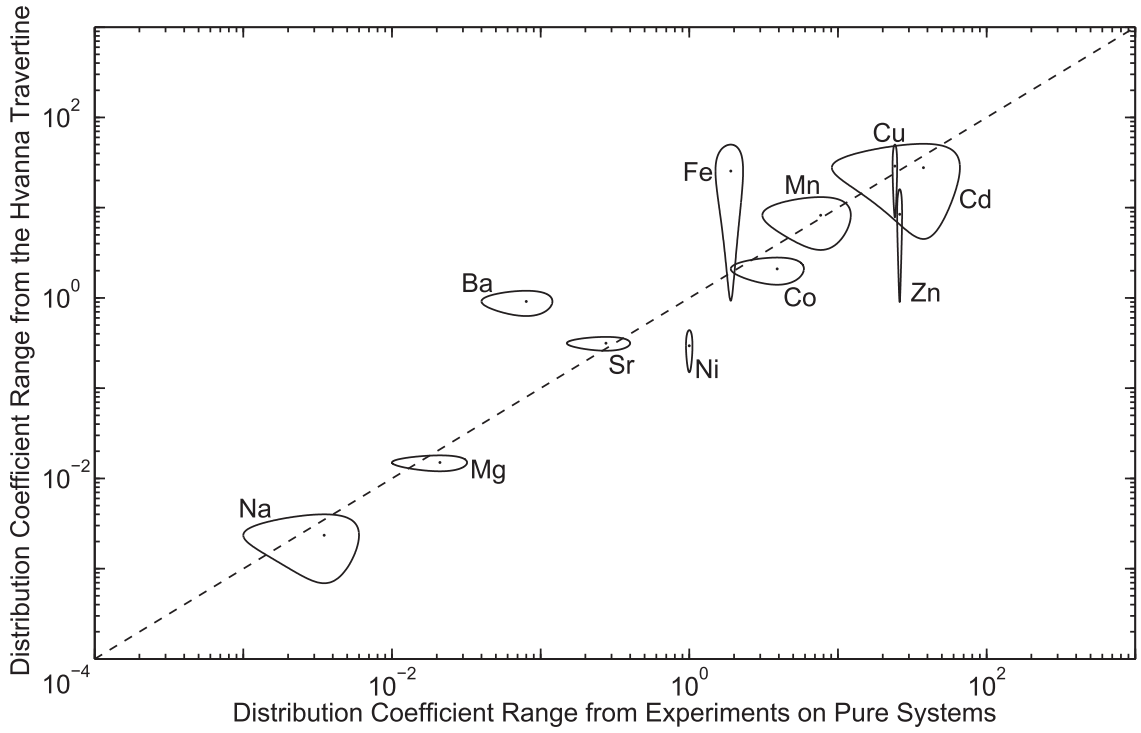

Fig. 8. The partition coefficients measured for the Hvanná River travertines versus data found in the literature that were derived from experiments on pure systems. The ellipse represents the range of values, defined by the p_{Me} average and range for each element listed in Table 3. The dot represents the average p_{Me}. The dotted line (1:1 p_{Me} ratio) can be used to assess the degree of correlation for partition coefficients from the natural travertine and the reported values from experiments on ideal systems.

rates. The goal of this part of the work was to identify the elements taken up by the calcite and to investigate the extent to which these are scavenged from the Hvanná River.

6.4.1. Evolution of the chemical composition downstream in the Hvanná River

The change in river water composition with distance downstream reflects a complicated combination of precipitation, coprecipitation, exchange and dissolution in addition to simple dilution. However, we can draw some conclusions by comparing concentrations of dissolved species. The elements that decrease most with distance downstream are associated with precipitating phases. These include Ba, Ca, Cd, Ce, Co, Cu, La, Mg, Mn, Nd, Ni, Pr, Sr, Zn and possibly Dy, Er, Gd, Sm and Yb (Fig. 3 and Table 2). Dissolved species that correlate with dissolved Ca concentration, and that were predicted to coprecipitate with calcite, include Ba, Co, Cu, Mg, Mn, Sr and possibly Cd, Na, Ni, P, Si, Ti and Zn (Table 3). The relatively lower linear correlation of dissolved Cd, Ni and Zn to Ca, compared with the other divalent ions suggests that these elements might be involved in other reactions or they might correlate with Ca in a nonlinear manner. Alternatively, Cd, Ni and Zn could have been scavenged completely as a result of their high partition coefficients and low concentrations in the Hvanná River. The concentration of dissolved elements, the oxygen level and pH are all variables that change with distance downstream and they affect the rate of coprecipitation for some elements. Calcium carbonates are known to take up small amounts of aqueous Si (Kitano et al., 1979; Klein and Walter, 1995; Belova et al., 2013) and P (Kitano et al., 1978; Neal, 2001). The good linear correlation of dissolved silica to calcium is probably a result of dilution downstream and of a very small fraction of Si uptake by calcite. The very rapid decrease of REE concentration with distance downstream indicates coprecipitation but too few samples had concentrations above the detection limit of the ICP-SFMS to be able to derive linear correlation coefficients (Fig. 3d). Previous studies have shown that calcite can take up a significant amount of REE (Terakado and Masuda, 1988; Zhong and Mucci, 1995; Stipp et al., 2006).

6.4.2. Chemical composition of the calcite

A wide range of elements was incorporated into the calcite. The mono- and divalent cations Mg^{2+}, Na^{+}, Mn^{2+} and Fe^{2+} were expected in calcite because they are known as common substitutes for Ca^{2+} in the atomic structure or in interstitial positions. Sulfate can substitute in small amounts for CO_3^{2-} in calcite and the uptake increases with the SO_4^{2-} to CO_3^{2-} ratio but decreases with the concentrations of Na and K (Kitano et al., 1975; Fernandez-Diaz et al., 2010). Kitano et al. (1975) reported that calcite precipitated in parent solutions containing 200 mg/L of SO_4^{2-} could scavenge about 14,500 ppm of sulfate, corresponding to 15 mmol per mole of calcite. This matches very well with the amount of incorporated sulfate found in the Hvanná calcite. The amount of Si associated with precipitated calcite matched well with a previous study (Kitano et al., 1979). Laboratory experiments conducted under similar conditions, i.e. Ca^{2+}: 8.5 mM, SiO_2: 0.42 to 1.7 mM, pH 7.5 to 8.2 at room temperature showed 1.6 to 67 μmol/(mole of calcite) compared with 60 to 87 μmol/(mole of calcite) in the travertine samples. The slightly higher uptake of the precipitated calcite in Hvanná can easily be explained by higher Na and Mg concentrations, which have been shown to increase the uptake of Si by carbonates (Kitano et al., 1979). The small amount of Si is likely to have deposited on grain boundaries of the dendrites rather than in crystal structure because the tetrahedral SiO_4^{4-} ion cannot substitute for the trigonal planar CO_3^{2-} ion. The Si values suggest that contamination by Si phases such as clays or ash particles and amorphous silica in the dissolved Hvanná samples was minimal. Other elements that are known to coprecipitate with calcite are Zn^{2+}, Ba^{2+}, La^{3+}, Ce^{3+}, Nd^{3+}, Gd^{3+}, Dy^{3+}, Co^{3+}, Pr^{3+}, Sm^{3+}, Ni^{2+}, Er^{3+}, Yb^{3+}, Cd^{2+}, Eu^{3+}, Ho^{3+} and Tb^{3+} (Zhong and Mucci, 1995; Rimstidt et al., 1998; Curti, 1999; Stipp et al., 2006) but Al also occurs in minor amounts and Ti, V, Tm and Lu in trace amounts in natural carbonate rocks (Turekian and Wedepohl, 1961). Some of these trace elements might be trapped in separate

phases located on grain boundaries in the calcite aggregates (discussed in Section 6.2) and then overgrown by further calcite precipitation.

The concentrations of Al, Ba, Fe, P, Ti and Zn were lower in the Hvanná River than in the water of the original, small Hvanná creek upstream from the mixing point (Site 1 in Fig. 1b). Increased concentration strongly suggests an influx of these elements from the small, freshwater creeks that mixed with the Hvanná River. The dissolved P concentration increased over the first 1300 m but decreased thereafter, in parallel with pH of the river water, reaching a stable level at 8.5 (Fig. 3 and Table 1). The initial increase of P in the river water indicates influx from sources other than the spring outlet, probably from smaller creeks.

Assuming that all the dissolved calcium from the flash dissolution experiments originated from calcite, we plotted the logarithmic concentrations per mole of calcite against distance downstream (Fig. 7). The concentration of Ba, Co, Mg, Mn, Na, Ni and Sr varies within an order of magnitude. These elements are associated with calcite, often as a solid solution (References in Table 3). Concentrations of Cd, Cu, Zn and the REE, most of which can also form solid solutions, also decrease both in the river water and in precipitated calcite with distance downstream. This indicates efficient scavenging by calcite, which limits the dissolved concentrations in the river water (Figs. 3 and 7). Pentecost (2005) suggested a simplified scenario for P in spring waters evolving from pH 7 to >8 along the flow path. According to Pentecost, coprecipitation of P in calcite increases with pH until all the dissolved P is adsorbed. In Hvanná, we observed a significant increase of P in the travertine along the flow path as pH increased (Figs. 3c and 7c). Concentrations of Al, Fe, Ni, Si and Ti in the precipitated travertine first decrease and then increase. This indicates that small amounts of clay and/or aluminum and iron hydroxide phases were dissolved along with the calcite in the flash dissolution experiments. However, since the concentrations of the other elements do not increase, these are expected mainly to originate from the travertine (Fig. 7).

6.4.3. Partition coefficients of the Hvanná calcite

The water composition in the Hvanná River was very stable over time. During our field trips over a span of more than three months, pH, Ca concentration, DIC and electrical conductivity varied by only 25% or less (Tables 1 and 2). Therefore, knowing the composition of both the river water and the precipitated calcite allowed us to determine partition coefficients for all the dissolved metals, using Eq. (1). These partition coefficients are presented in Table 3 together with values and reaction conditions for other studies reported in the literature. Our partition coefficients estimated for elements that commonly associate with calcium are in excellent agreement with the values from the literature, considering the complexity of the system. Fig. 8 shows a plot of the values derived from the travertines plotted as a function of the distribution coefficients derived from laboratory experiments on ideal systems.

The elements include Sr, Mn, Mg, Co and Cu, and to a lesser extent, Cd and Na. The distribution coefficient for Ba in travertine is a bit higher than from a pure system but this is undoubtedly because some barite ($BaSO_4$) has formed. This is likely because of the high S concentrations of the water. The value for Fe can be explained by the redox character. In these oxidizing waters, the iron would be present as Fe^{3+}, which does not fit into the calcite atomic structure. Uptake of iron is strongly correlated with the oxygen content of the samples, which increases downstream (Table 1). Iron is probably present in the travertine as ferrihydrite nanoparticles. A rough estimate from our data for the partition coefficients for La, Ce, Pr and Nd is 10. In data from laboratory studies (Curti et al., 2005) and natural calcites (Stipp et al., 2006), the partition coefficients for the REE vary from 10 to 1000, depending on the environment of formation and diagenesis. In work by Terakado and Masuda (1988), CO_2 was released from calcium bicarbonate solutions doped with REE until calcite precipitated. The precipitation coefficient obtained by this method ranged from 2.5 to 10 (Terakado and Masuda, 1988).

6.4.4. Formation of amorphous Ca–Mg carbonates?

The relative amount of calcium and magnesium removed from the Hvanná River is in the same order of magnitude; the concentrations decreased by 4.6 mM for calcium and 2.7 mM for magnesium. However, the calcite travertine deposits hold about 100 times more Ca than Mg, which indicates that Mg can coprecipitate in calcite but it could also form a secondary phase. No crystalline Mg phases or significant amount of amorphous material was detected with XRD. The Mg phase could have precipitated at a different location than the calcite or it could have been carried downstream by the river as small suspended particles. The river water was clear so heterogeneous nucleation, i.e. substrate catalyzed nucleation, is the predominant process in the Hvanná River, as is typical in nature. Homogeneous nucleation of calcite, i.e. spontaneous nucleation without a substrate, is only expected in solutions where the saturation index > 1 (Stumm, 1992; Lioliou et al., 2007). Homogeneous nucleation of Mg rich phases would require at least a similar degree of supersaturation.

Nesquehonite ($MgCO_3 \cdot 3H_2O$) has been observed to precipitate at 10 °C (Cheng and Li, 2009) and hydromagnesite ($Mg_5(CO_3)_4(OH)_2 \cdot 4H_2O$) can form at Earth surface conditions (Ming and Franklin, 1985; Cheng and Li, 2009). The river water of Hvanná was undersaturated with respect to these hydrated magnesium carbonates but precipitation of hydromagnesite, mediated by microorganisms, has previously been suggested (Braithwaite and Zedef, 1996; Power et al., 2009). Mg phases that were determined to be supersatured were magnesite (SI = 0.56), which requires temperatures above 80 °C to precipitate readily (Saldi et al., 2009), and the ordered Ca, Mg carbonate, dolomite (SI = 1.7), which does not form under conditions such as those of the Hvanná River. These carbonates have been synthesized in lab experiments at temperatures ranging from 40 to 60 °C but are not expected at lower temperatures (Deelman, 1999; Saldi et al., 2009).

Amorphous Ca, Mg carbonates are stable at high Mg:Ca ratios (Loste et al., 2003). Radha et al. (2012) synthesized a series of amorphous carbonates with composition $Ca_{1-x}Mg_xCO_3 \cdot nH_2O$ ($0 \le x \le 1$) at 4 °C by mixing solutions of $CaCl_2 \cdot 2H_2O$, $MgCl_2 \cdot 6H_2O$ and $NaCO_3$, which instantly formed a precipitate. The mixture concentrations were about a magnitude higher than the Mg and Ca concentrations in Hvanná. Amorphous calcium carbonates transform into calcite within hours while amorphous, Mg rich Ca carbonates can remain amorphous for more than a year, probably because of the more stable hydration state of magnesium (Radha et al., 2012). Radha et al. (2012) reported a partition coefficient for Mg of 0.44 for amorphous carbonates but a partition coefficient of 0.85 or higher is needed to account for complete loss of magnesium.

6.5. Implications for CO_2 immobilization

Coprecipitation of trace metals with carbonate minerals has important implications for the environment. One risk of immobilizing CO_2 by converting rocks such as basalt to secondary carbonate minerals is the potential release of toxic metals into drinking water, surface water or the environment. The goal of the CarbFix project is to trap CO_2 by forming stable carbonates in porous basaltic rocks, which when they dissolve, release the major divalent cations, Ca^{2+}, Mg^{2+} and Fe^{2+} but basalt dissolution also releases the heavy metals that are present in minor and trace concentrations in basaltic glass, the crystallized minerals and interstitial glass (Alfredsson et al., 2008; Gislason et al., 2010; Gislason and Oelkers, 2014).

Laboratory experiments, combined with model calculations (Flaathen et al., 2009; Galeczka et al., 2013a,b) and the study of natural analogues can provide background for predicting the final outcome of CO_2 injection in the short and long term. Selecting an appropriate natural analogue is not an easy task, as was discussed in detail by Bickle et al.

(2013). Perhaps the best documented natural examples of carbonation in basaltic rocks are: a low temperature (<125 °C) petroleum reservoir in West Greenland (Rogers et al., 2006), the high temperature (ambient to 300 °C) geothermal systems in Iceland (Wiese et al., 2008) and CO_2 charged ground waters (2–5 °C) in the vicinity of the Hekla volcano, Iceland (Flaathen et al., 2009). Mg–Fe rich carbonate minerals (magnesite to siderite) form at high partial pressure of CO_2, low temperature (<125 °C). Mg–Ca carbonates (dolomite) form at intermediate partial pressure and calcite forms at the lowest CO_2 pressure (Rogers et al., 2006). Calcite is also the dominant phase in high temperature geothermal basaltic systems and up to 70 kg CO_2 can be stored in a cubic meter of basaltic rock (Wiese et al., 2008). The CO_2 partial pressure of the carbonated ground waters in the vicinity of Hekla, Iceland was low; the in situ log pCO_2 was −2 to −4.5 bars and pH was between 6.9 to 9.2 (Flaathen et al., 2009). The concentration of toxic heavy metals in these waters was low and model calculations suggested that the metals had been incorporated into precipitated phases such as calcite and Fe(oxy)hydroxide (Flaathen et al., 2009). The identity of the phases that scavenged the metals was not known.

The travertine that formed in the Hvanná River provides the opportunity to explore which phases capture the toxic elements. The temperature was the same as for the Hekla waters but the partial pressure of CO_2 was slightly higher. However, in this study, the identity, composition and structure of the forming phases that scavenge the toxic metals could be investigated along the river flow path, downstream along a CO_2 partial pressure gradient. Of importance, the Hvanná River system can be considered as an analogue for the scenario where CO_2 charged waters leak to the surface from an injection site. The results provide confidence that toxic metals are trapped by secondary phases. At the Green River in Utah, natural CO_2 escaped from the subsurface and this system was recognized as a natural analogue for such a CO_2 leakage scenario (Bickle, 2009; Bickle et al., 2013; Kampman et al., 2014).

In the Hvanná River analogue, the groundwater was at calcite saturation as it emerged in the springs feeding the river (Fig. 6). The spring waters were loaded with metals and pH was 6.6. The pH had most likely risen from a value below 4, deep underground, in the vicinity of the intruded dike at Eyjafjallajökull (Fig. 1a). The increase resulted from dissolution of the basaltic host rock and dilution. In the Hvanná River, calcite precipitation is driven by CO_2 degassing and the ensuing increase of pH, causing supersaturation with respect to calcite (Fig. 6). This analogue study is directed to metal scavenging during pH increase from 6.6 to 8.5. All CO_2 charged waters that are injected into basalt follow this pH pathway as they migrate through the rock (Alfredsson et al., 2013). The increase in pH in the deep subsurface is driven by basalt dissolution and dilution rather than degassing as in the Hvanná River.

Coprecipitation coefficients derived from laboratory experiments are useful for indicating the extent of metal scavenging but the results are unlikely to reflect the true behavior of more complex, natural systems. Our study shows that the partition coefficients derived from laboratory experiments reported in the literature correspond well with values derived in the Hvanná River, a more realistic, natural system. This is important because the difference in crystallization rate, temperature, ionic strength, composition of the parent solution, particle size etc. has a limited effect on the metal absorption potential of calcite. Furthermore, the results justify the use of partition coefficients derived from simple solution in laboratory experiments in more complex systems relevant for carbon storage.

The amount of CO_2 potentially captured by calcite in the Hvanná River was estimated with the PHREEQC model. If the water equilibrated with the atmosphere and calcium only precipitated as calcite, 6.53 mmol of CO_2 per liter could be stored as $CaCO_3$. The discharge of the Hvanná River was approximately 0.44 m^3/s, corresponding to an annual CO_2 sequestration of $9.1 \cdot 10^7$ mol or approximately 4000 tonne of CO_2 in 9100 tonne of $CaCO_3$. This corresponds to 10% of the annual CO_2 emission from the Hellisheiði geothermal power plant at the CarbFix site in SW-Iceland (Alfredsson et al., 2013).

7. Conclusions

After the eruption of the Eyjafjallajökull volcano, a CO_2 outlet was discovered in the form of CO_2 charged spring water running from underneath the newly solidified lava. In addition to CO_2, the spring was heavily charged with many other dissolved constituents. The CO_2 that degassed from the water promoted pH increase and calcite precipitated as travertine in the stream bed. Precipitation rate was high, resulting in dendritic crusts and very porous material. Imperfect rhombohedral crystals were common and often overgrown by other crystal faces. Porous material had fine grained calcite arranged within box texture that probably originated from transformation of a metastable phase, probably the hydrated calcium carbonate, ikaite.

The decrease in concentration of the elements Cd, Co, Cu, Mg, Mn and Sr downstream in the Hvanná River correlated with the decrease of dissolved calcium. The partition coefficients derived for these elements matched extremely well with values reported in the literature. The partition coefficient estimated for Ba and Fe are higher than those reported from model system studies but this can be explained by the likely formation of barite and ferrihydrite in the travertine. Other elements were also taken up in the carbonate deposits, including, in order of abundance S, P, Al, K, Fe, Si, Ti, La, Ce, Nd, V, Gd, Dy, Pr, Sm, Er, Yb, Eu, Ho, Tb, Tm and Lu.

Other phases than calcite that were supersaturated in the Hvanná River and that might either directly precipitate or form secondary phases after basaltic rock weathering were silica, clay minerals, ferrihydrite and gibbsite. These phases could also have scavenged dissolved constituents from Hvanná but we were not able to identify any of them directly.

Our results have important implications for estimating the potential of calcite for scavenging toxic heavy metals in natural systems, in volcanic terrain and in engineered CO_2 injection systems in basaltic rocks, such as the CarbFix project. They provide evidence that the risk of release of toxic metals from CO_2 storage in basalt should be considered but if secondary carbonate phases are able to form, they are likely to sequester the metals, removing them from the water and minimizing the risk of transport in the environment.

Supplementary data to this article can be found online at http://dx.doi.org/10.1016/j.chemgeo.2014.06.025.

Acknowledgments

We thank Rósa Ólafsdóttir, Eydís Salome Eiríksdóttir, Kim Dalby, Helgi Alfreðsson, Helene Almind, Knud Dideriksen, Matthijs Arjen Smit, Tod Waight, Gro Birkefeldt and Iwona Gałeczka for their help and encouragement. For assistance in the field, we thank Anja Leth, Sam Scott, Simon Olsson and Sveinbjörn Steinþórsson. We are also grateful to two anonymous reviewers for their comments. The work was funded by the Nordic Volcanological Institute (NORDVULK), the Institute of Earth Sciences, Reykjavík, Iceland and the NanoGeoScience Group, Department of Chemistry, Copenhagen, Denmark.

References

Aiuppa, A., Allard, P., D'Alessandro, W., Michel, A., Parello, F., Treuil, M., Valenza, M., 2000a. Mobility and fluxes of major, minor and trace metals during basalt weathering and groundwater transport at Mt. Etna volcano (Sicily). Geochim. Cosmochim. Acta 64, 1827–1841.

Aiuppa, A., Dongarra, G., Capasso, G., Allard, P., 2000b. Trace elements in the thermal groundwaters of Vulcano Island (Sicily). J. Volcanol. Geotherm. Res. 98, 189–207.

Aiuppa, A., D'Alessandro, W., Federico, C., Palumbo, B., Valenza, M., 2003. The aquatic geochemistry of arsenic in volcanic groundwaters from southern Italy. Appl. Geochem. 18, 1283–1296.

Aiuppa, A., Federico, C., Allard, P., Gurrieri, S., Valenza, M., 2005. Trace metal modeling of groundwater–gas–rock interactions in a volcanic aquifer: Mount Vesuvius, Southern Italy. Chem. Geol. 216, 289–311.

Alexander, G.B., Heston, W.M., Iler, R.K., 1954. The solubility of amorphous silica in water. J. Phys. Chem. 58, 453–455.

Alfredsson, H.A., Hardarson, B.S., Franzson, H., Gislason, S.R., 2008. CO_2 sequestration in basaltic rock at the Hellisheidi site in SW Iceland: stratigraphy and chemical composition of the rocks at the injection site. Mineral. Mag. 72, 1–5.

Alfredsson, H.A., Oelkers, E.H., Hardarsson, B.S., Franzson, H., Gunnlaugsson, E., Gislason, S. R., 2013. The geology and water chemistry of the Hellisheidi, SW-Iceland carbon storage site. Int. J. Greenhouse Gas Control 12, 399–418.

Anthony, J.W., Bideaux, R.A., Bladh, K.W., Nichols, M.C.E., 2013. Handbook of Mineralogy. Mineralogical Society of America, Chantilly.

Aradottir, E.S.P., Sonnenthal, E.L., Bjornsson, G., Jonsson, H., 2012. Multidimensional reactive transport modeling of CO_2 mineral sequestration in basalts at the Hellisheidi geothermal field, Iceland. Int. J. Greenhouse Gas Control 9, 24–40.

Bachu, S., Gunter, W.D., Perkins, E.H., 1994. Aquifer disposal of CO_2: hydrodynamic and mineral trapping. Energy Convers. Manag. 35, 269–279.

Belova, D.A., Karaseva, O.N., Johnsson, A., Lakshtanov, L.Z., Stipp, S.L.S., 2014. Interaction between dissolved silica and calcite: part II — adsorption, coprecipitation and recrystallization. Geochim. Cosmochim. Acta (in revision).

Bickle, M.J., 2009. Geological carbon storage. Nat. Geosci. 2, 815–818.

Bickle, M., Kampman, N., Wigley, M., 2013. Natural analogues. Rev. Mineral. Geochem. 77, 15–71.

Bischoff, J.L., Fitzpatrick, J.A., Rosenbauer, R.J., 1993a. The solubility and stabilization of ikaite ($CaCO_3 \cdot 6H_2O$) from 0° to 25 °C: environmental and paleoclimatic implications for thinolite tufa. J. Geol. 101, 21–33.

Bischoff, J.L., Stine, S., Rosenbauer, R.J., Fitzpatrick, J.A., Stafford, T.W., 1993b. Ikaite precipitation by mixing of shoreline springs and lake water, Mono Lake, California, USA. Geochim. Cosmochim. Acta 57, 3855–3865.

Brady, P.V., Walther, J.V., 1990. Kinetics of quartz dissolution at low temperatures. Chem. Geol. 82, 253–264.

Braithwaite, C.J.R., Zedef, V., 1996. Hydromagnesite stromatolites and sediments in an alkaline lake, Salda Golu, Turkey. J. Sediment. Res. 66, 991–1002.

Busenberg, E., Plummer, L.N., 1985. Kinetic and thermodynamic factors controlling the distribution of SO_4^{2-} and Na^+ in calcites and selected aragonites. Geochim. Cosmochim. Acta 49, 713–725.

Busenberg, E., Plummer, L.N., 1986. A comparative study of the dissolution and crystal growth kinetics of calcite and aragonite. In: Mumpton, F.A. (Ed.), Studies in Diagenesis. US Geol. Surv. Bull, 1578, pp. 139–166.

Carrado, K.A., Decarreau, A., Petit, S., Bergaya, F., Lagaly, G., 2006. Chapter 4: Synthetic clay minerals and purification of natural clays. In: Bergaya, F., Theng, B.K.G., Lagaly, G. (Eds.), Handbook of Clay Science. Elsevier, Amsterdam, pp. 115–139.

Cheng, W., Li, Z., 2009. Precipitation of nesquehonite from homogeneous supersaturated solutions. Cryst. Res. Technol. 44, 937–947.

Chou, L., Wollast, R., 1985. Steady state kinetics and dissolution mechanisms of albite. Am. J. Sci. 285, 963–993.

Council, T.C., Bennett, P.C., 1993. Geochemistry of ikaite formation at Mono Lake, California: implications for the origin of tufa mounds. Geology 21, 971–974.

Curti, E., 1999. Coprecipitation of radionuclides with calcite: estimation of partition coefficients based on a review of laboratory investigations and geochemical data. Appl. Geochem. 14, 433–445.

Curti, E., Kulik, D.A., Tits, J., 2005. Solid solutions of trace Eu(III) in calcite: thermodynamic evaluation of experimental data over a wide range of pH and pCO_2. Geochim. Cosmochim. Acta 69, 1721–1737.

Deelman, J.C., 1999. Low-temperature nucleation of magnesite and dolomite. Neues Jahrb. Mineral. Monatshefte 289–302.

Dreybrodt, W., Buhmann, D., Michaelis, J., Usdowski, E., 1992. Geochemically controlled calcite precipitation by CO_2 outgassing: field measurements of precipitation rates in comparison to theoretical predictions. Chem. Geol. 97, 285–294.

Dromgoole, E.L., Walter, L.M., 1990. Iron and manganese incorporation into calcite — effects of growth-kinetics, temperature and solution chemistry. Chem. Geol. 81, 311–336.

Fernandez-Diaz, L., Fernandez-Gonzalez, A., Prieto, M., 2010. The role of sulfate groups in controlling $CaCO_3$ polymorphism. Geochim. Cosmochim. Acta 74, 6064–6076.

Flaathen, T.K., Gislason, S.R., Oelkers, E.H., Sveinbjornsdottir, A.E., 2009. Chemical evolution of the Mt. Hekla, Iceland, groundwaters: a natural analogue for CO_2 sequestration in basaltic rocks. Appl. Geochem. 24, 463–474.

Galeczka, I., Wolff-Boenisch, D., Gislason, S.R., 2013a. Experimental studies of basalt–H_2O–CO_2 interaction with a high pressure column flow reactor: the mobility of metals. Energy Procedia 37, 5823–5833.

Galeczka, I., Wolff-Boenisch, D., Jonsson, T., Sigfusson, B., Stefansson, A., Gislason, S.R., 2013b. A novel high pressure column flow reactor for experimental studies of CO_2 mineral storage. Appl. Geochem. 30, 91–104.

Galeczka, I., Wolff-Boenisch, D., Oelkers, E.H., Gislason, S.R., 2014. An experimental study of basaltic glass–H_2O–CO_2 interaction at 22 and 50 °C: implications for subsurface storage of CO_2. Geochim. Cosmochim. Acta 126, 123–145.

Gislason, S.R., Oelkers, E.H., 2003. Mechanism, rates, and consequences of basaltic glass dissolution: II. an experimental study of the dissolution rates of basaltic glass as a function of pH and temperature. Geochim. Cosmochim. Acta 67, 3817–3832.

Gislason, S.R., Oelkers, E.H., 2011. Silicate rock weathering and the global carbon cycle. In: Harmon, R., Parker, A. (Eds.), Frontiers in Geochemistry. John Wiley & Sons, Ltd, pp. 84–103.

Gislason, S.R., Oelkers, E.H., 2014. Carbon storage in basalt. Science 344, 373–374.

Gislason, S.R., Andrésdóttir, A., Steingrímsson, J.H., Jósavinsson, R.F., Ásbjörnsson, S., Rúnarsson, Þ., Stefánsson, A., Arnardóttir, G., Karlsdóttir, I., Friðriksson, Þ., 1995. Koltvísýringur frá Eyjafjallajökli, Eyjar í eldhafi. Gott mál, Reykjavík, pp. 229–234.

Gislason, S.R., Wolff-Boenisch, D., Stefansson, A., Oelkers, E.H., Gunnlaugsson, E., Sigurdardottir, H., Sigfusson, B., Broecker, W.S., Matter, J.M., Stute, M., Axelsson, G., Fridriksson, T., 2010. Mineral sequestration of carbon dioxide in basalt: a pre-injection overview of the CarbFix project. Int. J. Greenhouse Gas Control 4, 537–545.

Gislason, S.R., Hassenkam, T., Nedel, S., Bovet, N., Eiriksdottir, E.S., Alfredsson, H.A., Hem, C. P., Balogh, Z.I., Dideriksen, K., Oskarsson, N., Sigfusson, B., Larsen, G., Stipp, S.L.S., 2011. Characterization of Eyjafjallajökull volcanic ash particles and a protocol for rapid risk assessment. Proc. Natl. Acad. Sci. U. S. A. 108, 7307–7312.

Goldberg, D.S., Takahashi, T., Slagle, A.L., 2008. Carbon dioxide sequestration in deep-sea basalt. Proc. Natl. Acad. Sci. U. S. A. 105, 9920–9925.

Gran, G., 1952. Determination of the equivalence point in potentiometric titrations. Part II. Analyst 77, 661–671.

Hammer, O., Jamtveit, B., Benning, L.G., Dysthe, D.K., 2005. Evolution of fluid chemistry during travertine formation in the Troll thermal springs, Svalbard, Norway. Geofluids 5, 140–150.

Hammer, O., Dysthe, D.K., Jamtveit, B., 2007. The dynamics of travertine dams. Earth Planet. Sci. Lett. 256, 258–263.

Ito, T., 1996. Ikaite from cold spring water at Shiowakka, Hokkaido, Japan. J. Mineral. Petrol. Econ. Geol. 91, 209–219.

Jamtveit, B., Hammer, O., Andersson, C., Dysthe, D.K., Heldmann, J., Vogel, M.L., 2006. Travertines from the Troll thermal springs, Svalbard. Nor. J. Geol. 86, 387–395.

Kampman, N., Bickle, M.J., Maskell, A., Chapman, H.J., Evans, J.P., Purser, G., Zhou, Z., Schaller, M.F., Gattacceca, J.C., Bertier, P., Chen, F., Turchyn, A.V., Assayag, N., Rochelle, C., Ballentine, C.J., Busch, A., 2014. Drilling and sampling a natural CO_2 reservoir: implications for fluid flow and CO_2–fluid–rock reactions during CO_2 migration through the overburden. Chem. Geol. 369, 51–82.

Kelemen, P.B., Matter, J., 2008. In situ carbonation of peridotite for CO_2 storage. Proc. Natl. Acad. Sci. U. S. A. 105, 17295–17300.

Kerr, P.F., 1952. Formation and occurrence of clay minerals. Clays and Clay Miner. 1, 19–32.

Kitano, Y., Okumura, M., Idogaki, M., 1975. Incorporation of sodium, chloride and sulfate with calcium carbonate. Geochem. J. 9, 75–84.

Kitano, Y., Okumura, M., Idogaki, M., 1978. Uptake of phosphate ions by calcium carbonate. Geochem. J. 12, 29–37.

Kitano, Y., Okumura, M., Idogaki, M., 1979. Behavior of dissolved silica in parent solution at the formation of calcium carbonate. Geochem. J. 13, 253–260.

Kitano, Y., Okumura, M., Idogaki, M., 1980. Abnormal behaviors of copper(II) and zinc ions in parent solution at the early stage of calcite formation. Geochem. J. 14, 167–175.

Klein, R.T., Walter, L.M., 1995. Interactions between dissolved silica and carbonate minerals: an experimental study at 25–50 °C. Chem. Geol. 125, 29–43.

Köhler, S.J., Dufaud, F., Oelkers, E.H., 2003. An experimental study of illite dissolution kinetics as a function of pH from 1.4 to 12.4 and temperature from 5 to 50 °C. Geochim. Cosmochim. Acta 67, 3583–3594.

Krauskopf, K.B., 1956. Dissolution and precipitation of silica at low temperatures. Geochim. Cosmochim. Acta 10, 1–26.

Lackner, K.S., Wendt, C.H., Butt, D.P., Joyce, E.L., Sharp, D.H., 1995. Carbon dioxide disposal in carbonate minerals. Energy 20, 1153–1170.

Lakshtanov, L.Z., Stipp, S.L.S., 2007. Experimental study of nickel(II) interaction with calcite: adsorption and coprecipitation. Geochim. Cosmochim. Acta 71, 3686–3697.

Larsen, D., 1994. Origin and paleoenvironmental significance of calcite pseudomorphs after ikaite in the Oligocene Creede Formation, Colorado. J. Sediment. Res. A64, 593–603.

Lioliou, M.G., Paraskeva, C.A., Koutsoukos, P.G., Payatakes, A.C., 2007. Heterogeneous nucleation and growth of calcium carbonate on calcite and quartz. J. Colloid Interface Sci. 308, 421–428.

Lorens, R.B., 1981. Sr, Cd, Mn and Co distribution coefficients in calcite as a function of calcite precipitation rate. Geochim. Cosmochim. Acta 45, 553–561.

Loste, E., Wilson, R.M., Seshadri, R., Meldrum, F.C., 2003. The role of magnesium in stabilising amorphous calcium carbonate and controlling calcite morphologies. J. Cryst. Growth 254, 206–218.

Lovering, T.G., Patten, L.E., 1962. The effect of CO_2 at low temperature and pressure on solutions supersaturated with silica in the presence of limestone and dolomite. Geochim. Cosmochim. Acta 26, 787–790.

Lu, G., Zheng, C., Donahoe, R.J., Lyons, W.B., 2000. Controlling processes in a $CaCO_3$ precipitating stream in Huanglong Natural Scenic District, Sichuan, China. J. Hydrol. 230, 34–54.

McGrail, B.P., Schaef, H.T., Ho, A.M., Chien, Y.J., Dooley, J.J., Davidson, C.L., 2006. Potential for carbon dioxide sequestration in flood basalts. J. Geophys. Res. Solid Earth 111.

McGrail, B.P., Spane, F.A., Sullivan, E.C., Bacon, D.H., Hund, G., 2011. The Wallula basalt sequestration pilot project. Energy Procedia 4, 5653–5660.

Meakin, P., Jamtveit, B., 2010. Geological pattern formation by growth and dissolution in aqueous systems. Proc. R. Soc. A 466, 659–694.

Ming, D.W., Franklin, W.T., 1985. Synthesis and characterization of lansfordite and nesquehonite. Soil Sci. Soc. Am. J. 49, 1303–1308.

Morse, J.W., Bender, M.L., 1990. Partition coefficients in calcite: examination of factors influencing the validity of experimental results and their application to natural systems. Chem. Geol. 82, 265–277.

Mucci, A., Morse, J.W., 1983. The incorporation of Mg^{2+} and Sr^{2+} into calcite overgrowths: influences of growth rate and solution composition. Geochim. Cosmochim. Acta 47, 217–233.

Neal, C., 2001. The potential for phosphorus pollution remediation by calcite precipitation in UK freshwaters. Hydrol. Earth Syst. Sci. 5, 119–131.

Oelkers, E.H., Gislason, S.R., Matter, J., 2008. Mineral carbonation of CO_2. Elements 4, 333–337.

Okumura, M., Kitano, Y., 1986. Coprecipitation of alkali metal ions with calcium carbonate. Geochim. Cosmochim. Acta 50, 49–58.

Olsson, J., Bovet, N., Makovicky, E., Bechgaard, K., Balogh, Z., Stipp, S.L.S., 2012. Olivine reactivity with CO_2 and H_2O on a microscale: implications for carbon sequestration. Geochim. Cosmochim. Acta 77, 86–97.

Olsson, J., Stipp, S.L.S., Dalby, K.N., Gislason, S.R., 2013. Rapid release of metal salts and nutrients from the 2011 Grímsvötn, Iceland volcanic ash. Geochim. Cosmochim. Acta 123, 134–149.

Omelon, C.R., Pollard, W.H., Marion, G.M., 2001. Seasonal formation of ikaite ($CaCO_3 \cdot 6H_2O$) in saline spring discharge at Expedition Fiord, Canadian High Arctic: assessing conditional constraints for natural crystal growth. Geochim. Cosmochim. Acta 65, 1429–1437.
Parkhurst, D.L., Appelo, C.A.J., 1999. User's guide to PHREEQC (version 2) — a computer program for speciation, batch-reaction, one-dimensional transport, and inverse geochemical calculations. U.S. Geological Survey Water Resources Investigation Report, pp. 99–4259.
Pauly, H., 1963. 'Ikaite', a new mineral from Greenland. Arctic 16, 263–264.
Pedersen, R., Sigmundsson, F., 2004. InSAR based sill model links spatially offset areas of deformation and seismicity for the 1994 unrest episode at Eyjafjallajokull volcano, Iceland. Geophys. Res. Lett. 31.
Pedersen, R., Sigmundsson, F., 2006. Temporal development of the 1999 intrusive episode in the Eyjafjallajokull volcano, Iceland, derived from InSAR images. Bull. Volcanol. 68, 377–393.
Pentecost, A., 2005. Travertine. Springer, London.
Pingitore, N.E., Eastman, M.P., 1984. The experimental partitioning of Ba^{2+} into calcite. Chem. Geol. 45, 113–120.
Pokrovsky, O.S., Schott, J., 2000. Kinetics and mechanism of forsterite dissolution at 25 °C and pH from 1 to 12. Geochim. Cosmochim. Acta 64, 3313–3325.
Power, I.M., Wilson, S.A., Thom, J.M., Dipple, G.M., Gabites, J.E., Southam, G., 2009. The hydromagnesite playas of Atlin, British Columbia, Canada: a biogeochemical model for CO_2 sequestration. Chem. Geol. 260, 286–300.
Power, I.M., Wilson, S.A., Dipple, G.M., 2013. Serpentinite carbonation for CO_2 sequestration. Elements 9, 115–121.
Radha, A.V., Fernandez-Martinez, A., Hu, Y.D., Jun, Y.S., Waychunas, G.A., Navrotsky, A., 2012. Energetic and structural studies of amorphous $Ca_{1-x}Mg_xCO_3 \cdot nH_2O$ ($0 \le x \le 1$). Geochim. Cosmochim. Acta 90, 83–95.
Rimstidt, J.D., Balog, A., Webb, J., 1998. Distribution of trace elements between carbonate minerals and aqueous solutions. Geochim. Cosmochim. Acta 62, 1851–1863.
Rogers, K.L., Neuhoff, P.S., Pedersen, A.K., Bird, D.K., 2006. CO_2 metasomatism in a basalt-hosted petroleum reservoir, Nuussuaq, West Greenland. Lithos 92, 55–82.
Saldi, G.D., Jordan, G., Schott, J., Oelkers, E.H., 2009. Magnesite growth rates as a function of temperature and saturation state. Geochim. Cosmochim. Acta 73, 5646–5657.
Schwertmann, U., Cornell, R.M., 2000. Iron Oxides in the Laboratory: Preparation and Characterization. Wiley, Weinheim.
Seifritz, W., 1990. CO_2 disposal by means of silicates. Nature 345, 486.
Shearman, D.J., Smith, A.J., 1985. Ikaite, the parent mineral of jarrowite-type pseudomorphs. Proc. Geol. Assoc. 96, 305–314.
Shearman, D.J., McGugan, A., Stein, C., Smith, A.J., 1989. Ikaite, $CaCO_3 \cdot 6H_2O$, precursor of the thinolites in the Quaternary tufas and tufa mounds of the Lahontan and Mono Lake basins, western United States. Geol. Soc. Am. Bull. 101, 913–917.
Sigmarsson, O., Vlastelic, I., Andreasen, R., Bindeman, I., Devidal, J.L., Moune, S., Keiding, J. K., Larsen, G., Höskuldsson, A., Thordarson, T., 2011. Remobilization of silicic intrusion by mafic magmas during the 2010 Eyjafjallajökull eruption. Solid Earth 2, 271–281.
Sigmundsson, F., Hreinsdottir, S., Hooper, A., Arnadottir, T., Pedersen, R., Roberts, M.J., Oskarsson, N., Auriac, A., Decriem, J., Einarsson, P., Geirsson, H., Hensch, M., Ofeigsson, B.G., Sturkell, E., Sveinbjornsson, H., Feigl, K.L., 2010. Intrusion triggering of the 2010 Eyjafjallajökull explosive eruption. Nature 468, 426–430.
Stefansson, A., Gislason, S.R., 2001. Chemical weathering of basalts, Southwest Iceland: effect of rock crystallinity and secondary minerals on chemical fluxes to the ocean. Am. J. Sci. 301, 513–556.
Stipp, S.L.S., Christensen, J.T., Lakshtanov, L.Z., Baker, J.A., Waight, T.E., 2006. Rare Earth element (REE) incorporation in natural calcite: upper limits for actinide uptake in a secondary phase. Radiochim. Acta 94, 523–528.
Stumm, W., 1992. Chemistry of the Solid–Water Interface: Processes at the Mineral–Water and Particle–Water Interface in Natural Systems. Wiley, New York.
Stumm, W., Morgan, J.J., 1981. Aquatic Chemistry: an Introduction Emphasizing Chemical Equilibria in Natural Waters. Wiley, New York.
Suess, E., Balzer, W., Hesse, K.F., Muller, P.J., Ungerer, C.A., Wefer, G., 1982. Calcium carbonate hexahydrate from organic-rich sediments of the antarctic shelf: precursors of glendonites. Science 216, 1128–1131.
Terakado, Y., Masuda, A., 1988. The coprecipitation of rare earth elements with calcite and aragonite. Chem. Geol. 69, 103–110.
Turekian, K.K., Wedepohl, K.H., 1961. Distribution of the elements in some major units of the earth's crust. Geol. Soc. Am. Bull. 72, 175–192.
Wiese, F., Fridriksson, T., Armannsson, H., 2008. CO_2 Fixation by Calcite in High-temperature Geothermal Systems in Iceland. Iceland Geosurvey, Reykjavík.
Winkler, L.W., 1888. Die Bestimmung des im Wasser gelösten Sauerstoffes. Ber. Dtsch. Chem. Ges. 21, 2843–2854.
Zhong, S.J., Mucci, A., 1995. Partitioning of rare earth elements (REEs) between calcite and seawater solutions at 25 °C and 1 atm, and high dissolved REE concentrations. Geochim. Cosmochim. Acta 59, 443–453.